NA

REPORT DOCUMENTATION PAGE

Form Approved
OMB No. 0704-0188

1. AGENCY USE ONLY (Leave blank)	2. REPORT DATE	3. REPORT TYPE AND DATES COVERED
	31 JUL 1995	Final Report, 1 DEC 1992 - 31 MAY 1995

4. TITLE AND SUBTITLE
Transient Shear Layer Dynamics of Two- and Three-Dimensional Open Cavities

5. FUNDING NUMBERS
F49620-93-1-0081

AFOSR-TR-95

0505

6. AUTHOR(S)
Dr. Paul D. Orkwis
Dr. Peter J. Disimile

7. PERFORMING ORGANIZATION NAME(S) AND ADDRESS(ES)
University of Cincinnati
Dept. AsE & EM
Cincinnati, OH 45221-0070

REPORT NUMBER
N/A

9. SPONSORING / MONITORING AGENCY NAME(S) AND ADDRESS(ES)
AFOSR/NA
Building 410
Bolling AFB
Washington, DC 20332-6448

NA

10. SPONSORING / MONITORING AGENCY REPORT NUMBER
F49620-93-1-0081

11. SUPPLEMENTARY NOTES
The view, opinions and/or findings contained in this report are those of the author(s) and should not be construed as an official Department of the Air Force position, policy, or decision, unless so designated by other documentation.

12a. DISTRIBUTION / AVAILABILITY STATEMENT
Approved for public release; distribution unlimited.

12b. DISTRIBUTION CODE

13. ABSTRACT *(Maximum 200 words)*
An experimental and computational research effort was performed to investigate the flow physics inherent in supersonic open cavities. Experiments were performed on a 2:1 length to depth ratio, 12:1 aspect ratio cavity at a Mach number of 2 and a Reynolds number based on momentum thickness of 3.69×10^4. Wind tunnel velocity profiles were obtained for use as inflow boundary conditions in the computations. Time averaged and time unsteady surface pressure data were taken and analyzed for spectral frequency content and compared to Rossiter's experimental/empirical formula. Computations were made at the experimental conditions and results compared with the experimental data. A detailed comparison of results obtained will all reported cavity modifications of the Baldwin-Lomax turbulence model was performed to determine which simulated best both time averaged and time unsteady properties. Time histories of flow fields were obtained and compared to the oscillation cycle descriptions of Rockwell and Naudascher, and Heller and Bliss. Results indicate qualitative agreement with the former but considerable differences with the latter. Recommendations are made for obtaining improved simulations and greater understanding of the flow physics.

14. SUBJECT TERMS	15. NUMBER OF PAGES
Supersonic Open Cavities, Computational Fluid Dynamics, Experimental Fluid Dynamics, Turbulence Modeling, Acoustic Oscillations, Unsteady Fluid Dynamics, Flow Physics	78
	16. PRICE CODE

17. SECURITY CLASSIFICATION OF REPORT	18. SECURITY CLASSIFICATION	19. SECURITY CLASSIFICATION OF ABSTRACT	20. LIMITATION OF ABSTRACT
UNCLASSIFIED	UNCLASSIFIED	UNCLASSIFIED	UL

Final Technical Report

Transient Shear Layer Dynamics of Two- and Three-Dimensional Open Cavities

by

Dr. Paul D. Orkwis

and

Dr. Peter J. Disimile

University of Cincinnati

Contract Period
12/1/92 - 5/31/95

AFOSR Grant # F49620-93-1-0081

Contract Monitor

Dr. Leonidas Sakell

Abstract

An experimental and computational research effort was performed to investigate the flow physics inherent in supersonic open cavities. Experiments were performed on a 2:1 length to depth ratio, 12:1 aspect ratio cavity at a Mach number of 2 and a Reynolds number based on momentum thickness of $3.69x\,10^4$. Wind tunnel velocity profiles were obtained for use as inflow boundary conditions in the computations. Time averaged and time unsteady surface pressure data were taken and analyzed for spectral frequency content and compared to Rossiter's empirical formula. Computations were made at the experimental conditions and results compared with the experimental data.. A detailed comparison of results obtained with all reported cavity modifications of the Baldwin-Lomax turbulence model was performed to determine which simulated best both time averaged and time unsteady properties. Time histories of flow fields were obtained and compared to the oscillation cycle descriptions of Rockwell and Naudascher, and Heller and Bliss. Results indicate qualitative agreement with the former but considerable differences with the latter. Recommendations are made for obtaining improved simulations and greater understanding of the flow physics.

Introduction

The fundamental details of three dimensional supersonic open cavity flow fields are of interest to the Air Force because cavities will be a part of any future high speed stealthy attack, fighter or reconnaissance aircraft. Increased drag, high heat transfer rates and structurally damaging oscillations are all associated with these flow fields. In addition, the requirement for launching stores from such an environment makes an understanding of the fundamental large and small scale flow field details vital to the success of any new military aircraft concept.

The basic physical structure of cavity flow fields can be described as either closed, open or transitioning[1 2 3 4] . Closed cavities are typically long and shallow with a length to depth ratio (L/D) greater than 13. They are characterized by a shear layer that impinges on the cavity floor producing two large recirculation regions. Closed cavities are associated with high drag coefficients[5 6 7 8] and heat transfer properties[9 10 11 12] as compared to open cavities, as such, they are less desirable. Open cavities are short and deep with an L/D less than 10. They contain shear layers that span the cavity and are more typical of those found in aircraft applications. Open cavity flow fields are remarkably complicated with internal and external regions that are coupled via self sustained shear layer oscillations. Coherent shed vorticity, unsteady weak shock or pressure waves, and interactions between the shed vortices and the vortices that reside in the cavity are also present. Flow field characteristics appear to depend primarily upon the shape of the cavity and the Mach number, with Reynolds number effects considered to be less important.

Although there have been numerous investigations into these flow fields, very little fundamental knowledge of the flow physics has been obtained that is more than qualitative. Several issues remain to be understood for open cavity flow fields. Researchers appear to agree that an oscillating shear layer exists, that the primary and secondary vortices residing within the cavity are driven by the shear layer, that a mass "breathing" effect occurs within the cavity, and that pressure oscillations exist. However, the mechanisms driving this flow field have not yet been agreed upon.

Notable experimental efforts by Rossiter[13], Rockwell et al.[14 15], and Heller and Bliss[16] have attempted to determine some of these details. Rossiter employed dimensional analysis and empiricism to produce the following formula for the cavity resonance

frequencies

$$f = \frac{U}{L}\frac{(m - \gamma)}{\left(\frac{1}{K} + M\right)}$$

Where U is the freestream velocity, L is the cavity length, M is the Mach number, m is an integer (1,2,3, ...), and γ and K are constants. Rossiter's formula predicts the dominant frequency of the cavity oscillation with remarkable accuracy. This number can also be obtained from numerical simulations and is one of the more appropriate accuracy metrics for this unsteady flow. Rossiter's model was derived using an edge tone analogy and the assumption that the acoustic radiation is due to shed vortices impinging on the aft cavity wall. His experiments visualized the shed vortices and the pressure waves external to the cavity, although they did not visualize the standing waves described as existing within the cavity. This work laid the foundation for the more comprehensive theories regarding cavity resonance put forth by Heller and Bliss[16], and Rockwell and Naudascher[15].

Rockwell et al. and others[14 15 17] provide an explanation of the cavity resonance cycle which stipulates that the shear layer oscillation is driven primarily by transient vortex motions within the cavity. They contend that the vortices which form within the oscillating shear layer sometimes impinge upon the aft wall and then mix with vortices inside the cavity. The shear layer vortex/edge interaction adds mass to the cavity; the "breathing-in" phase. This captured vortex then interacts with the internal cavity vortices, displacing them and producing pressure oscillations within the cavity. These fluctuations travel forward and eventually displace the shear layer at the leading edge. This produces an external excitation of the shear layer that initiates the shedding of another vortex and closes the feedback loop.

A second mechanism, proposed by Heller and Bliss[16] and cited by several other researchers[18 19], defines the shear layer oscillation cycle as dependent upon unsteady planar compression waves. Once again the cycle begins with the unstable shear layer detaching from the trailing edge and impinging on the aft wall of the cavity. Mass enters the cavity in a fashion similar to the previous explanation. A normal shock

wave forms and is convected upstream. This shock wave is accompanied by an inviscid region shock wave which equalizes the pressure across the shear layer. The internal shock eventually hits the forward wall and is reflected back into the cavity. The pressure doubling behind the reflected shock displaces the shear layer and initiates a new shed vortex. The reflected shock passes through new forward moving shocks as it travels towards the aft wall. The inviscid region shock wave no longer exists since the external flow is subsonic relative to the internal shock wave motion. The cycle is completed when the reflected shock hits the aft wall; expelling mass from the cavity in the "breathing out" phase.

It should be noted that although the two descriptions appear to be quite different, the two points of view are not mutually exclusive. The current research has produced evidence that indicates there is some truth to both explanations.

Previous Air Force and Air Force sponsored researchers investigating the above cycles have produce considerable computational evidence regarding the nature of the cavity resonance cycle. Hankey and Shang[18], Rizzetta[19], Tu[20], Suhs[21], and Baysal and Stallings[22], have all attempted to simulate the open cavity resonance cycle. All of these efforts employed a RANS approach with an algebraic turbulence model. More advanced turbulence models, such as one and two equation models, have also been attempted. The general results indicate that a wide variety of solutions are obtained with the various turbulence models. Good results are typically obtained for time averaged surface properties like pressure and shear stress, but unsteady properties like sound pressure levels (SPLs) and cavity resonance frequency are not computed consistently. This is perhaps not surprising since turbulence models are not typically tuned to unsteady applications.

This final report details the current research investigation into the supersonic open cavity oscillation cycle flow physics. A joint experimental/computational approach was taken as detailed in the following sections. Included are descriptions of the experimental testing apparatus, the computational algorithm, the general research approach, the implementation of the approach, findings from the research and recommendations regarding future directions.

Experimental Apparatus

To provide insight into the flow physics of open cavities and data for code validation an experimental component was undertaken, using a single deep cavity. A streamwise length to depth ratio (L/D) of 2 was used as a representative open cavity shape. Thereby, two-dimensional results were obtained by using a relatively high aspect ratio (lateral width to streamwise length, (W/L)) cavity of approximately 12:1 placed in a supersonic flow.

The primary piece of hardware is the University of Cincinnati's supersonic wind tunnel. This tunnel is of an intermittent blowdown configuration. The test section is 15.24 cm. wide (6 in.) by 16.54 cm. tall (6.5 in.). The Mach numbers in the tunnel can be varied between 1.4 and 3.8 through the use of an asymmetric nozzle block arrangement. Reynolds numbers between 27.6 to 82.7 million per meter can be realized in the tunnel Mach number range. Figure 1 provides a diagrammatic sketch of the supersonic wind tunnel facility.

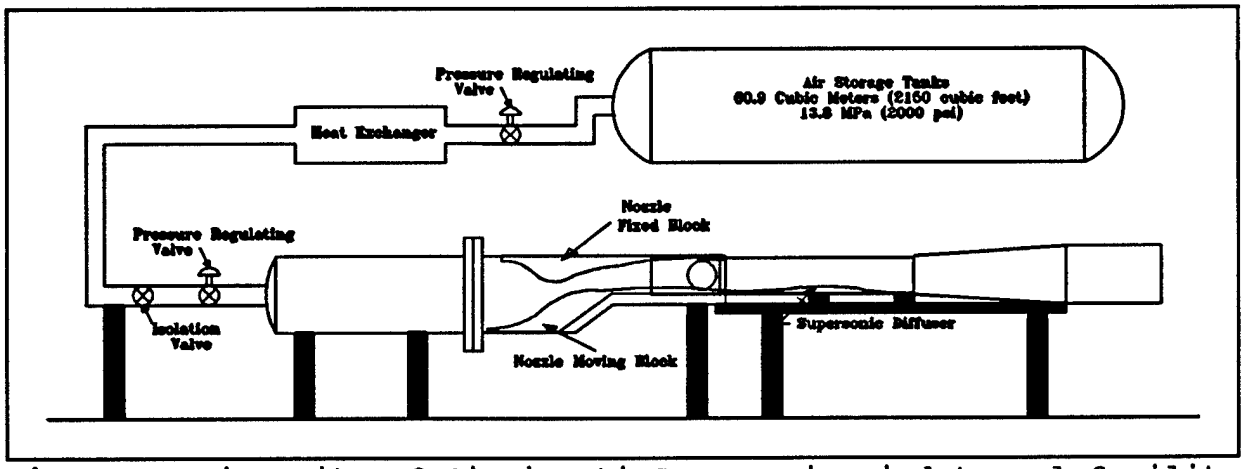

Figure 1 University of Cincinnati Supersonic wind tunnel facility

The wind tunnel is supplied by four compressed air storage tanks containing 60.9 m^3 (2150 ft^3) of gas at pressures reaching 13.6 Mpa (2000 psi). Upon exiting the storage tank the air is directed into a heat exchanger which is used to maintain air temperature stability. Using two pressure regulators the air is permitted to fill the stagnation plenum, immediately upstream of the supersonic nozzle, while maintaining a constant stagnation pressure.

The tunnel data acquisition system is centered around a PC microcomputer with a commercially available data acquisition system. The software was written in such a way that the tunnel parameters are displayed in pseudo-real time, both graphically and numerically. The tunnel acquisition computer is a 12 MHz 286, therefore, allowing the display to be updated every 20 seconds. The tunnel parameters measured include the manifold, stagnation and static pressures along with heat exchanger air-in and air-out temperatures, as well as, the stagnation temperature (Figure 2).

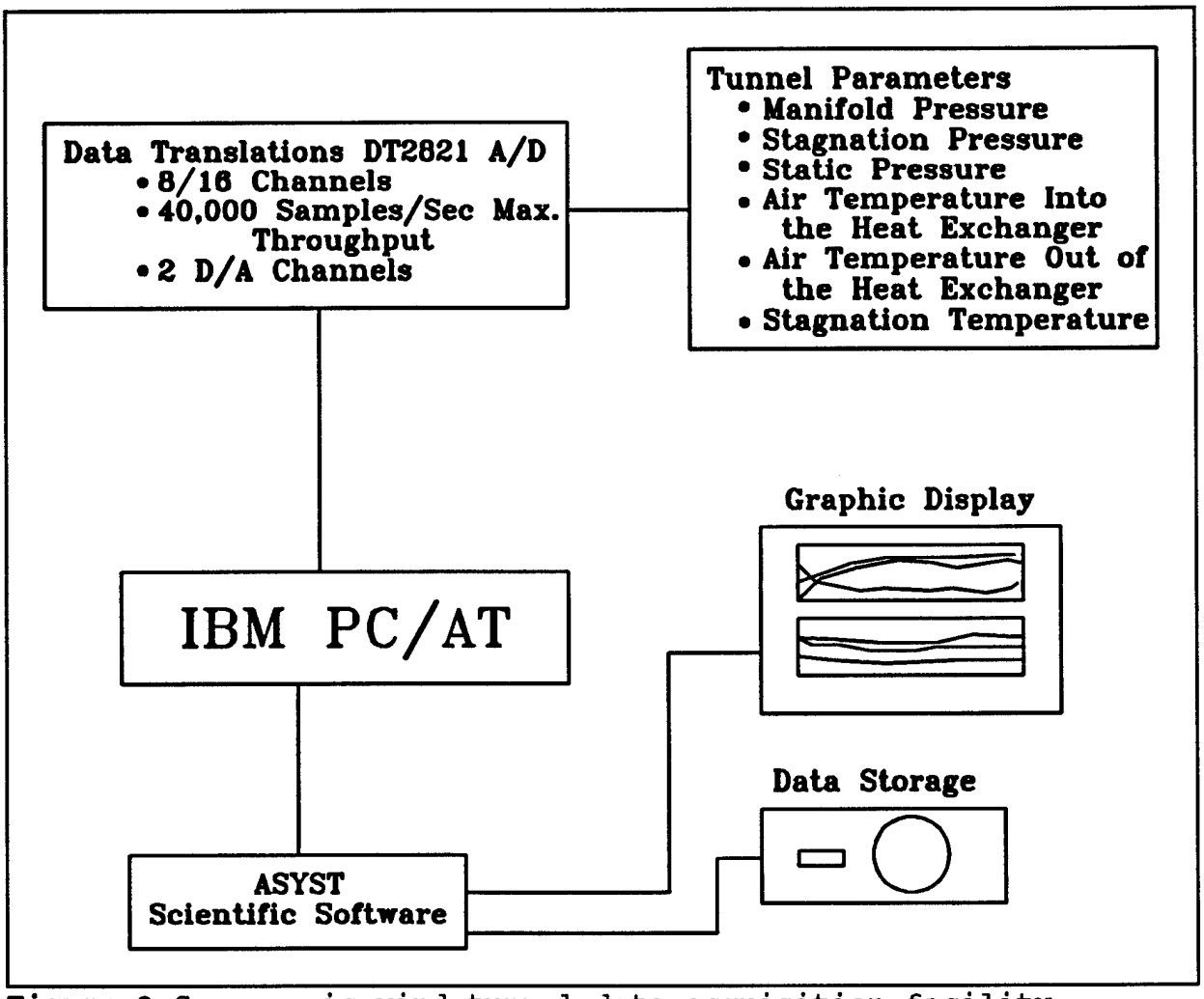

Figure 2 Supersonic wind tunnel data acquisition facility

The Cavity Model

As shown in figure 3, the cavity consists of a segmented circular aluminum plug with a rectangular aluminum insert. The plug diameter is 17.78 cm (7 in.). The rectangular opening in the cavity floor has dimensions of 12.38 cm (4.875 in.) by 1.05 cm (0.412 in.). This results in an aspect ratio of 11.83. The aluminum insert which creates the floor for the cavity is 1.27 cm (0.5 in.) thick and is adjustable to provide for different L/D ratios between 0.5 and 2. For the current configuration, the L/D ratio was 2.

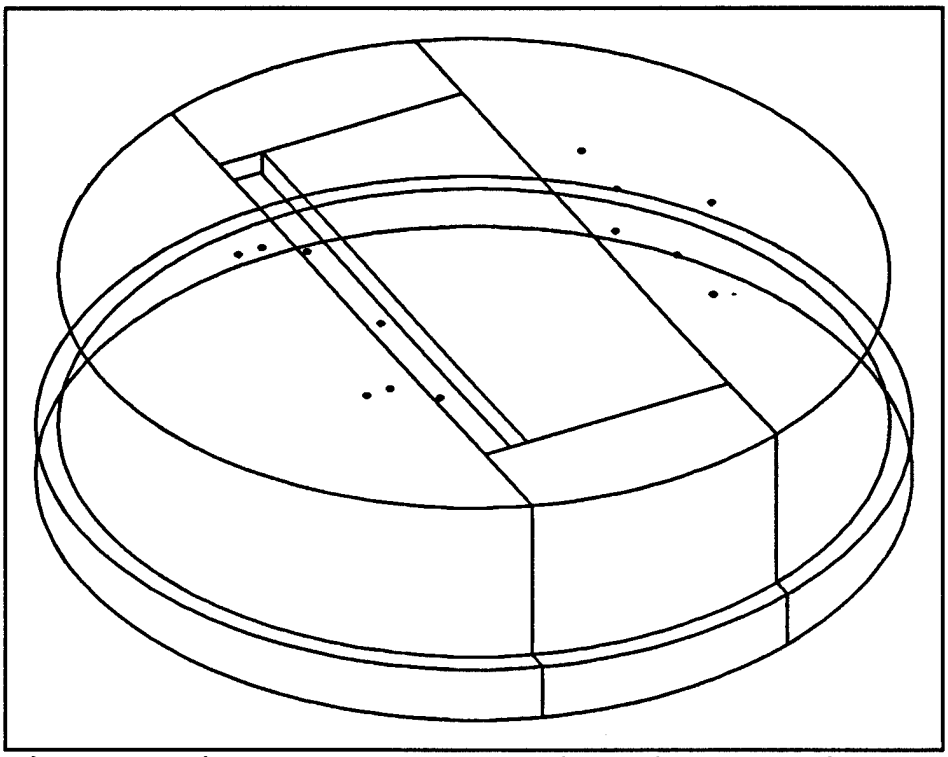

Figure 3 Diagram of the two dimensional cavity model

F o r
averaged surface pressure measurements, 34 surface taps are located throughout the model (Figure 4). Locations included the upstream boundary layer, the cavity region, and the aft lip of the model. To check for two-dimensionality, taps were located 2.03 cm (0.8 in.) from either side of the centerline and 0.24 cm (0.093 in.) below the plug surface.

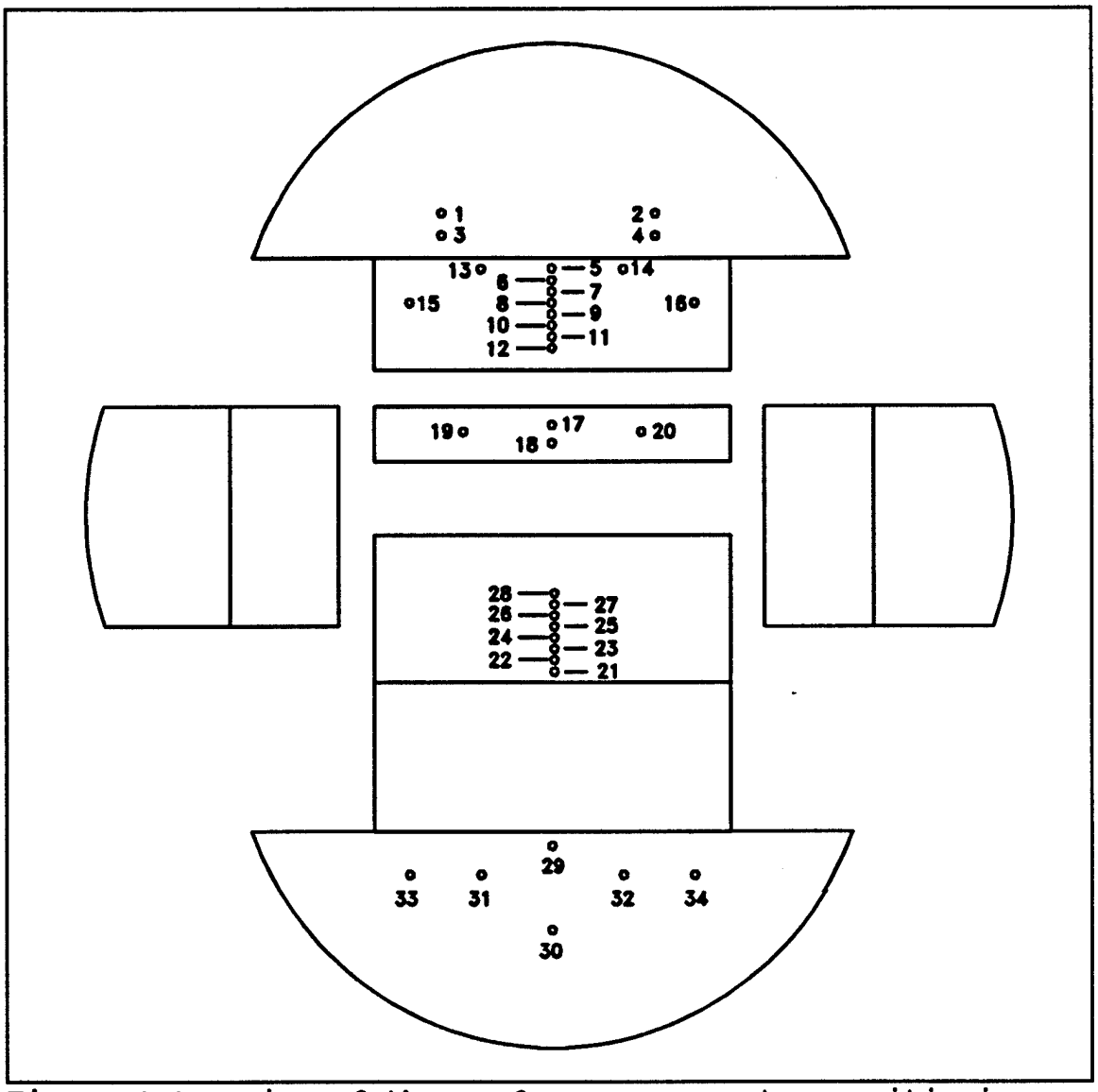

Figure 4 Overview of the surface pressure tap positioning

Also mounted in the cavity model are three high speed pressure transducers. The first transducer is mounted at the separation lip while a second is mounted on the floor of the cavity approximately 0.66L downstream from the separation lip. The third and last high speed transducer was mounted on the aft lip of cavity (see fig.). The transducers have a resonant frequency of 125 kHz and a usable range of 25 KHz (as per the manufacture). Each transducer had a matched amplifier calibrated at the factory to be +/- 2%. The transducer outputs were digitized using an 8 channel 16 bit simultaneous sample and hold A/D convertor and processed using a 486 based micro-computer (see Figure 5).

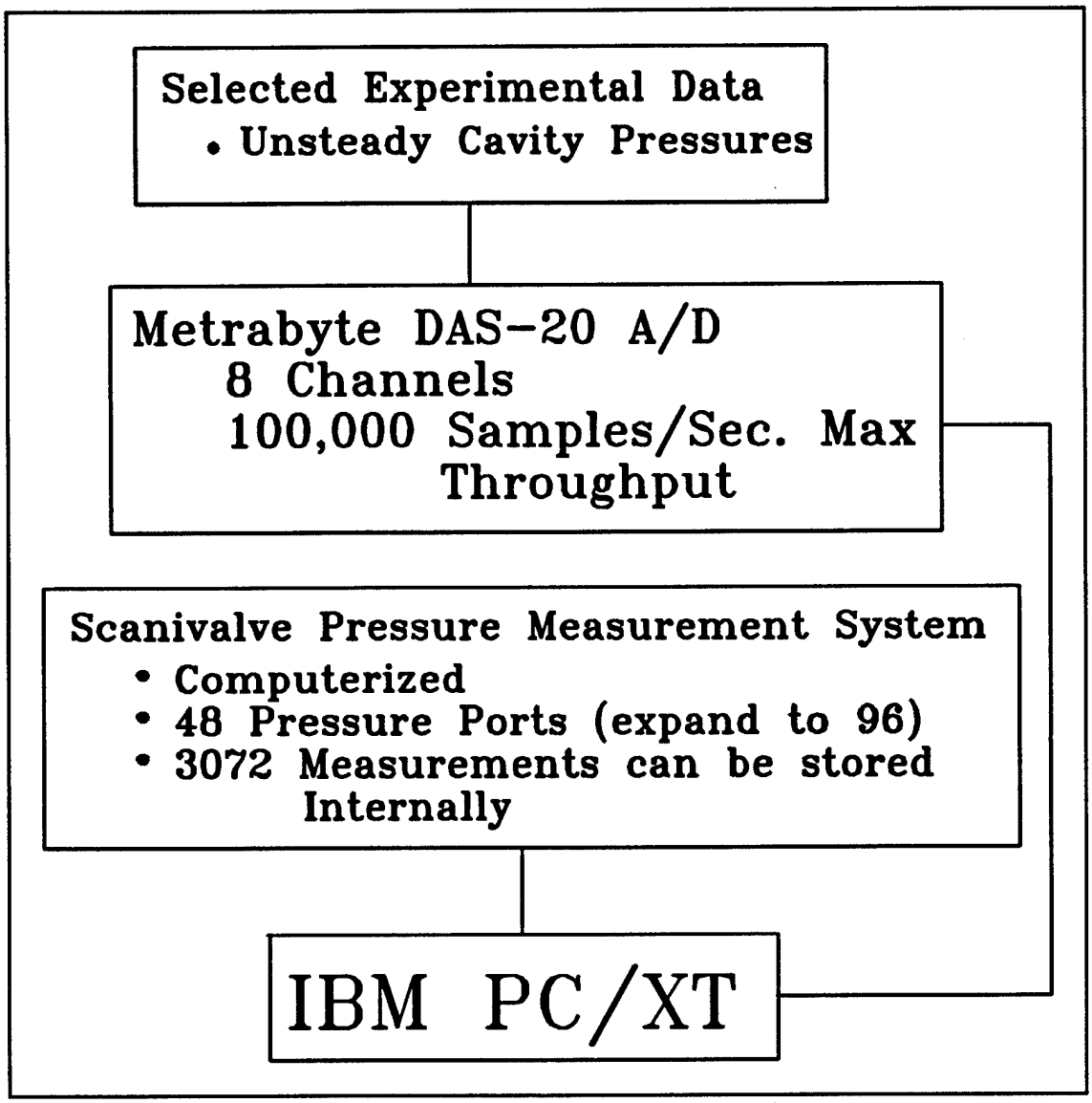

Figure 5 Unsteady pressure measurement system

In the present study steady state surface pressure data were acquired at a rate of 200 Hz. Unsteady surface pressures were acquired at a sampling rate of 50 KHZ.

Computational Algorithm

The implicit upwind finite volume scheme of Simpson and Whitfield[23] was employed in this work. The original scheme was applied to pitching airfoil problems and solved the three-dimensional thin-layer Navier-Stokes equations. The code was modified in the current work by adding viscous terms in the axial direction, thus producing the double-thin-layer Navier-Stokes equations. The residuals for this scheme are formed via Roe's flux difference splitting and achieve third order accuracy in the spatial direction using the techniques developed by Osher and Chakravarthy. The Van Albada limiter was used to prevent nonphysical oscillations near discontinuities, while approximate factorizations were used to solve the resultant system of equations.

The linearized implicit form of the discrete governing equations can be split into flux vectors with either non-negative (indicated by a plus superscript) or non-positive eigenvalues (indicated by a minus superscript). Appropriate upwind differencing gives the approximate implicit scheme

$$(I + \Delta\tau\nabla_\xi A^+ + \Delta\tau\nabla_\eta B^+ + \Delta\tau\nabla_\zeta C^+ + \Delta\tau\Delta_\xi A^- + \Delta\tau\Delta_\eta B^- + \Delta\tau\Delta_\zeta C^-)\Delta Q^n = -\Delta\tau R^n$$

where

$$R^n = -\Delta\tau\left(\frac{\partial F^n}{\partial\xi} + \frac{\partial G^n}{\partial\eta} + \frac{\partial H^n}{\partial\zeta} + \frac{\partial S^n{}_v}{\partial\eta}\right)$$

The system of equations can then be written as an approximate system of the form

$$(I + \Delta\tau\nabla_\xi A^+ + \Delta\tau\nabla_\eta B^+ + \Delta\tau C^+)*$$
$$(I + \Delta\tau\Delta_\xi A^- + \Delta\tau\Delta_\eta B^- + \Delta\tau\Delta_\zeta C^-)\Delta Q^n = -\Delta\tau R^n$$

The flux Jacobians in the above equation are then obtained from the Steger-Warming flux vector splitting, and the residual vector, R^n, from Roe's flux difference splitting.

The solution to system of equations is found in the following manner.

$$(I + \Delta\tau \nabla_\xi A^+ + \Delta\tau \nabla_\eta B^+ + \Delta\tau \Delta_\zeta C^+)X = -\Delta\tau R^n$$
$$(I + \Delta\tau \Delta_\xi A^- + \Delta\tau \Delta_\eta B^- + \Delta\tau \Delta_\zeta C^-)X^2 = X^1$$
$$\Delta Q^n = X^2$$

The above equations require the solution to two systems of equations. The first system is solved in a forward pass, resulting in a lower block bi-diagonal system, and the second system is solved by a backward pass, resulting in an upper block bi-diagonal system. The solution of the equations gives the desired solution vector, $\Delta^n Q$, from which the dependent variable vector at time level n+1 can be obtained

$$\Delta Q^{n+1} = Q^n + \Delta^n Q$$

The resulting numerical method can be run using local timestepping for steady state problems or second order accurate in time by employing a Newton like subiteration procedure for unsteady problems. This procedure can be thought of as a pseudotime iteration which recovers full temporal accuracy after pseudotime convergence. Acceptable convergence is typically obtained with four subiterations and frozen Jacobians, as shown by Simpson and Whitfield. The implementation of the subiterations in the algorithm can be easily described by considering the following temporally first order algorithm

$$(I + \Delta\tau \nabla_\xi A^+ + \Delta\tau \nabla_\eta B^+ + \Delta\tau \nabla_\zeta C^+) *$$
$$(\Delta\tau \Delta_\xi A^- + \Delta\tau \Delta_\eta B^- + \Delta\tau \Delta_\zeta C^-)\Delta Q^p = RHS^p$$

where

$$RHS^p = -\Delta\tau\left[\frac{Q^p - Q^n}{\Delta\tau} + \left(\frac{\partial F^p}{\partial\xi} + \frac{\partial G^p}{\partial\eta} + \frac{\partial H^p}{\partial\zeta}\right)\right]$$

with ΔQ^p defined as

$$\Delta Q^p = Q^p - Q^{p-1}$$

and p a subiteration counter. At convergence $Q^p \rightarrow Q^{n+1}$, and the viscous terms are no longer lagged.

Second order temporal accuracy can be achieved by employing data at additional time levels and appropriate temporal differences.

Initial and Boundary Conditions

Initial and boundary conditions are set as described in the first journal article resulting from this work by Orkwis, Tam and Disimile[24]. A flat plate computation was performed to produce a boundary layer with momentum thickness identical to that found in the experiment. The inflow conditions were set identical to the next to last column of the flat plate computation. Outflow conditions were specified as exptrapolated variables as they were supersonic.

Initial conditions outside of the cavity were set everywhere equal to the inflow profiles. Density and pressure within the cavity were set equal to the surface condition of the inflow profile. Velocities within the cavity were set to one half their respective freestream values. Energy was then determined based on the other variables.

Grids

Grids were chosen based on a brief grid resolution study and the results of other researchers. The minimum y^+ based on the inflow profile was 4.4. Three grid blocks were employed so that no grid interface would exist through the shear layer. The upstream block was dimensioned 66x55 cells, the cavity block 66x120 cells and the downstream block 66x55 cells. A total of 15,180 cells were employed. Points were

clustered along all walls using the function

$$x_p = \frac{e^{-k\left(\frac{j}{N}-1\right)} - 1}{e^{k} - 1}$$

where j is the point index and N is the total number of points in a column (row).

Turbulence Models

One significant result of this research involves a comparison of the solutions obtained with several algebraic turbulence models employed by previous researchers for cavity simulations. The following describes the basic algebraic turbulence model used in the work, its various modifications and two laminar flow simulations.

Fully Laminar (FL)

The simplest approach to modeling the turbulence is to ignore it. That was done in the fully laminar (FL) model in which flow for all three blocks was assumed to be laminar.

Laminar In And Above The Cavity (LIA)

The next method in complexity is to assume laminar flow in the cavity block only. The upstream and downstream blocks are computed using the standard Baldwin-Lomax turbulence model discussed next.

Standard Baldwin-Lomax (SBL)

The standard Baldwin-Lomax [25] turbulence model is an algebraic model that has become a workhorse for many computations. It employs a two-layer algebraic eddy viscosity model in which μ_t is given by

$$\mu_t = \begin{cases} (\mu_t)_{inner} & y \le y_{crossover} \\ (\mu_t)_{outer} & y_{crossover} \le y \end{cases}$$

where y is the normal distance from the wall and $y_{crossover}$ is the smallest y value at which values from the inner and outer formulas match. The formula for the inner region is based on the Prandtl-Van Driest eddy viscosity

$$(\mu_t)_{inner} = \rho l^2 |\omega|$$

with

$$l = ky\left[1 - \exp\left(-\frac{y^+}{A^+}\right)\right]$$

where $|\omega|$ is the magnitude of the vorticity and

$$y^+ = \frac{\rho_w u_\tau y}{\mu_w} = \frac{\sqrt{\rho_w \tau_w} y}{\mu_w}$$

The outer region is defined from the Clauser formulation

$$(\mu_t)_{outer} = KC_{CP}\rho F_{wake} F_{Kleb}(y)$$

where K is the Clauser constant, C_{CP} is an additional constant, F_{Kleb} is the Klebanoff intermittency factor

$$F_{Kleb}(y) = \left[1 + 5.5\left(\frac{C_{Kleb} y}{y_{Max}}\right)^6\right]^{-1}$$

and F_{wake} is found from

$$F_{wake} = \min \begin{cases} y_{Max} F_{Max} \\ \dfrac{C_{WK} Y_{Max} u^2_{Dif}}{F_{Max}} \end{cases}$$

with the quantities y_{Max} and F_{Max} determined based on the maximum value of the function

$$F(y) = y|\omega| \left[1 - \exp\left(-\frac{y^+}{A^+} \right) \right]$$

Additional parameters are

$$u_{Dif} = (\sqrt{u^2 + v^2 + w^2})_{Max} - (\sqrt{u^2 + v^2 + w^2})_{Min}$$

and the constants

$$A^+ = 26, \quad C_{CP} = 1.6, \quad C_{Kleb} = 0.3$$
$$C_{WK} = 0.25, \quad k = 0.4, \quad K = 0.0168$$

This model is simple and practical, hence it is used extensively. However, it does have some limitations with regard to cavity flows. The reference length changes abruptly from the upstream flat plate to the cavity. Consequently, an abrupt discontinuity results in the eddy viscosity. In addition, the model computes the eddy viscosity based only on a profile and not with regard to up- or downstream flow conditions. To counter these deficiencies several researchers have modified the basic model as discussed below.

Relaxation Modification (REL)

The abrupt x direction change in eddy viscosity from the upstream flat plate into the cavity region is eliminated by the relaxation modification. This technique was first

applied by Shang and Hankey[26] in the study of a supersonic compression ramp. IN this scheme, the SBL model is used to compute the initial values of the eddy viscosity. The actual values are then calculated from

$$\mu_t = \mu_{tw} + (\mu_{sbl} - \mu_{tu})\left[1 - \exp\left(-\frac{x}{10\,\delta}\right)\right]$$

where μ_{sbl} is the unaltered SBL viscosity, μ_{tu} is the upstream turbulent viscosity at the cavity lip, δ is the instantaneous boundary layer thickness at the upstream corner, and x is the streamwise distance from the corner. This modification has been shown to work well in numerical calculations of compression corner flows with separation by Visbal and Knight[27]. It produces a weighted average of the local eddy viscosity with the upstream value, thereby producing a continuous variation of μ_t in the x-direction.

First Peak Modification (FP)

Alluded to in the last section is the difficulty in choosing the appropriate reference length, which directly affects the computation of $(\mu_t)_{outer}$. In recirculation regions, the function F(y) has multiple peaks, therefore, there is some ambiguity regarding the proper maximum of F. A larger peak caused by the overlying vortex structure can be found in addition to the peak due to the attached boundary layer. Choice of the second (larger) peak results in an outer region viscosity that is larger than that obtained by choosing the first maxima. Choice of the first peak results in an approach that is typically attributed to Digenea and Schiff[28]. Its general effect is to reduce the overall eddy viscosity throughout most of the shear layer. It is applied in this work only in the cavity. It had been applied previously in cavity simulations by Baysal[29].

Multiple Wall Modification (MW)

This modification takes account of the effects from all walls within the cavity in an approach employed by Gorski, Ota and Chakravarthy[30], and Baysal, Yen, and Fouladi[31]. This is accomplished through an inverse averaging approach to compute the eddy viscosity values based on profiles normal to all three walls. The total eddy viscosity is found from

$$\mu_t = \frac{\dfrac{\mu_{t_{w1}}}{y^+_1} + \dfrac{\mu_{t_{w2}}}{y^+_2}}{\sqrt{\left(\dfrac{1}{y^+_1}\right)^2 + \left(\dfrac{1}{y^+_2}\right)^2}}$$

where μ_{tw_1} is the turbulent viscosity obtained by applying the Baldwin-Lomax model normal to wall 1 and μ_{tw_2} is that obtained from wall 2, etc. This formulation allows the wall with the lower y^+ value (usually the closest wall) to be relatively more important than the neighboring wall. This technique is applied in the cavity using the two vertical walls and the floor to compute the eddy viscosity.

Suhs' Modification (SU)

Suhs[20] investigated 3-D open cavities using the SBL model applied on the upstream and downstream flat plate regions and in the cavity, but not above the cavity.

Inverse Suhs' Modification (ISU)

Since Suhs model does not at first glance appear physically realistic, it was decided to test the inverse of this approach. That is, the SBL applied in the upstream and downstream flat plate regions and the region above but outside the cavity, with no model used inside the cavity.

The above eight models were tested in the current research.

Approach

The general research approach taken in this effort was a combined experimental and computational exercise. In this way the strengths of each approach offset the weaknesses of the other. In particular, the experimental work would provide initial insight into the flow physics and valuable evidence to validate the computations. The computations would provide full field data to gain insight into particular flow physics mechanisms in a temporally resolved way that experiments are unable to reproduce. The computations were made with boundary data that "matched" the experiment as described earlier; i.e. a Mach number 2.0, Reynolds number (based on momentum thickness) of $3.69x\,10^4$, a momentum thickness of 0.979 mm. The cavity had a 2:1 length to depth ratio and a 12:1 length to width ratio. These dimensions were prescribed to simulate a two-dimensional flow.

The experiments consisted primarily of pressure data; both time averaged and time resolved. In addition, an effort was undertaken to develop an LV capability for later use in determining velocity profiles within the field. Time averaged pressure data were obtained at many stations along the surface of the cavity geometry. Time resolved pressure data was obtained at three locations on the surface; the upstream flat plate region, the floor of the cavity and the downstream flat plate region.

Computations were performed for the above conditions. The computations were run six characteristic times to purge startup transients and reach a "steady" oscillating flow. Data was sampled at each iteration along the cavity surface for later spectral analysis and comparison with experiment. Field data was sampled at a lower frequency because of the enormous disk storage requirements. A similar set of data was obtained for each of the eight turbulence models.

The initial work determined the "best" approach for turbulence modeling (of the models tested) based on comparison with the experiments. The results from that approach were then studied to ascertain the flow physics inherent in the cavity. Profiles of the time averaged pressure were compared and the spectral content of the pressure on the cavity flow computed to compare with Rossiter's prediction of fundamental frequency. The approach that "best" fit to all of these criterion was then studied further.

Field data of the vorticity and instantaneous streamlines were plotted to investigate the flow field details and compare with the vortex interaction oscillation cycle proposed by Rockwell and Naudascher[15]. Field data of the pressure were also plotted to compare with Heller and Bliss'[16] pressure wave oscillation cycle description. Animations of these data were made and movies created to observe the features in a dynamic sense.

The implementation of the above approach is discussed in the next section followed by the results obtained from these results.

Implementation

EXPERIMENTAL BOUNDARY CONDITIONS

The wind tunnel test parameters for the present study were set to $M_\infty = 2$, $Re_\theta = 3.69 \times 10^4$ and $L/D = 2$. A traversing total pressure probe was then employed to measure the Mach number distribution across the test section. The probe, through the use of various attachments, was able to measure the total pressure at the centerline, 2.54 cm (1 inch) and 5.08 cm (2 inches) above and below the centerline. The local Mach number was then calculated using the Raleigh-pitot formula.

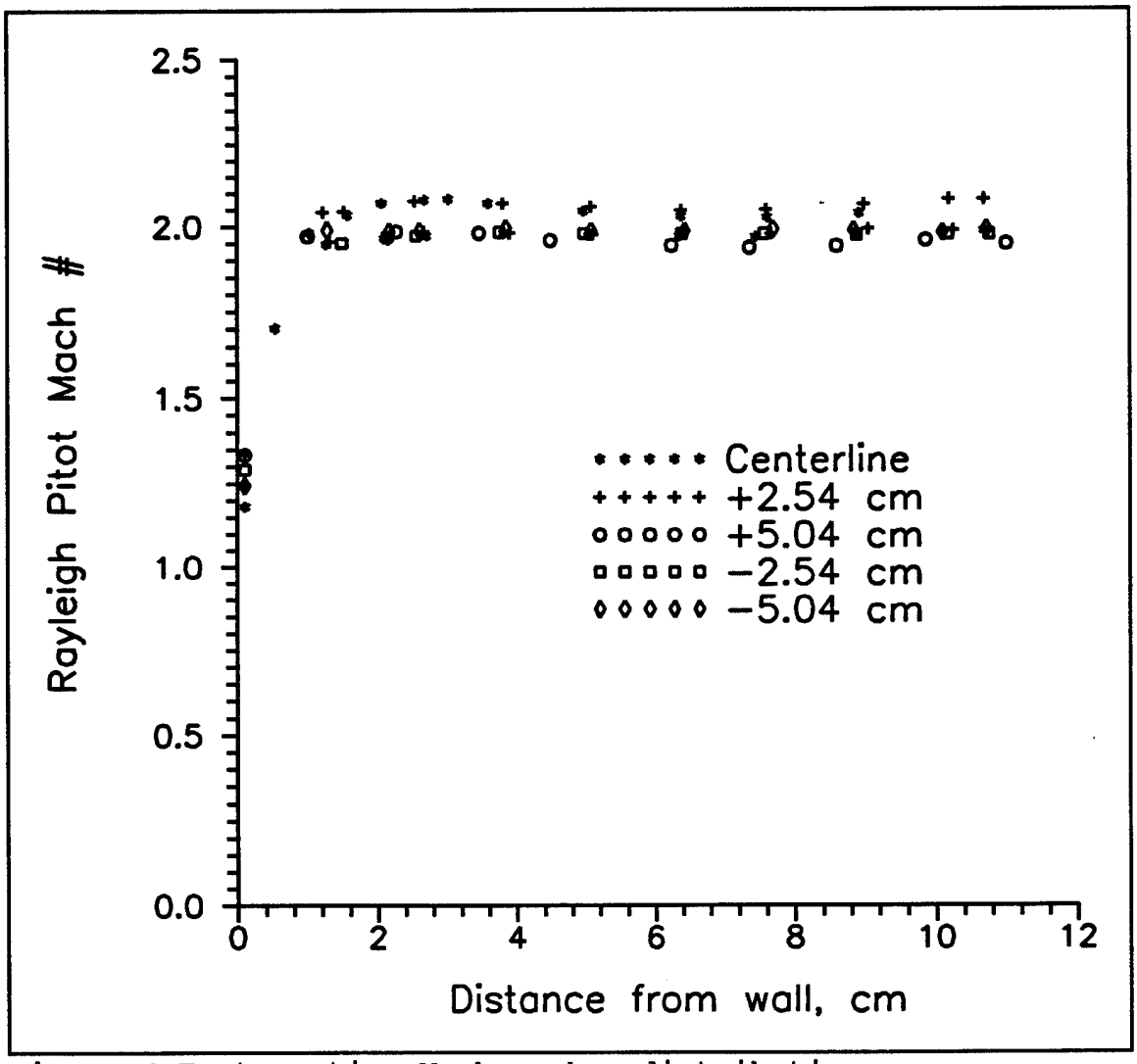

Figure 6 Test section Mach number distribution

Figure 6 shows the test section Mach number variation from the near wall to approximately 3.79 cm (1.5 inches) from the far wall for all five positions. The overall averaged freestream Mach number within the test section core was 1.98 +/- 0.06. The boundary layer velocity profile for the same locations was also obtained. The boundary layer thickness was estimated to be approximately 1.27 cm. To verify repeatability several centerline boundary layer traverses were obtained. Figure 7 displays the velocity profile obtained from four separate centerline tests.

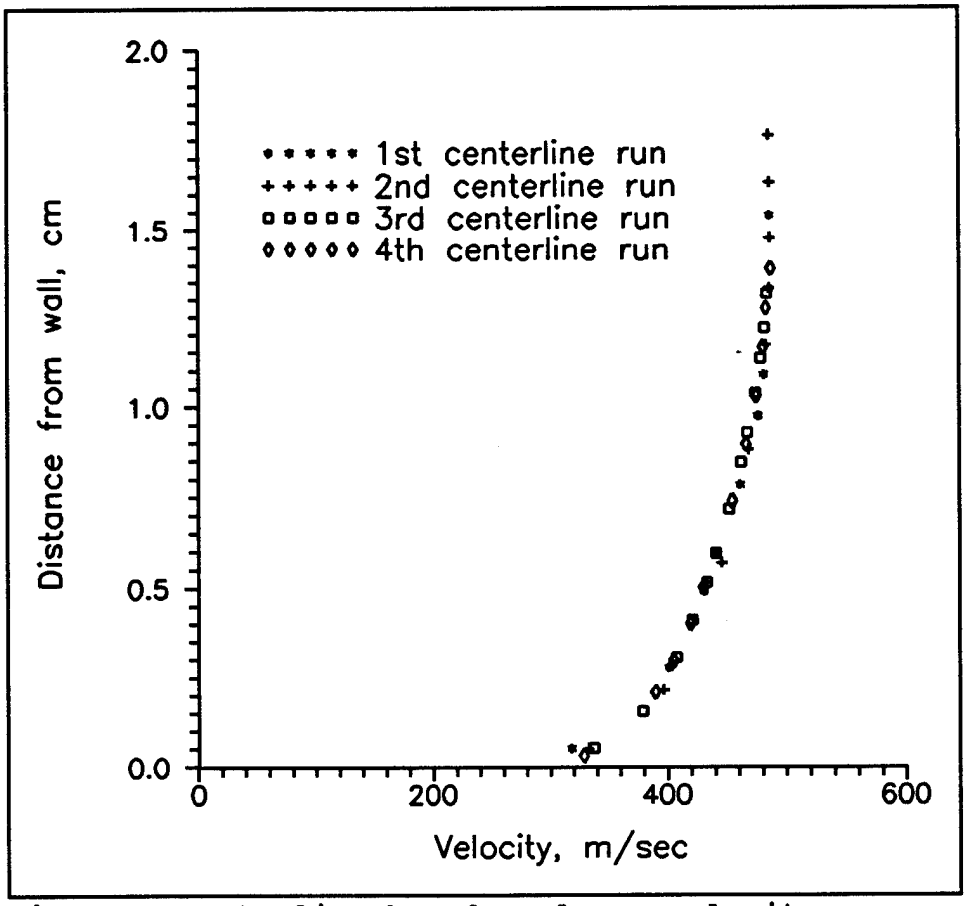

Figure 7 Centerline boundary layer velocity distribution

The data from the centerline and positions below the centerline compare rather well. The worst case velocity deviation throughout the boundary layer was 7%. When a Power Law profile was fit to the data, the exponent was 8.4. Replotting in wall coordinates, the data showed good agreement with the Law of The Wall in the range of $250 < y+ < 25{,}000$ with a skin friction coefflcient (cf) of 0.0020. Also as a comparison, the Van Driest transformation was performed on the velocity profile and

the C_f recalculated. The skin friction for this case was 0.0021. The boundary layer momenturn thickness was calculated to be 9.79 mm. with a lateral variation of less than 20%. Figure 8 is a comparison of the experimentally acquired data and the power law fit.

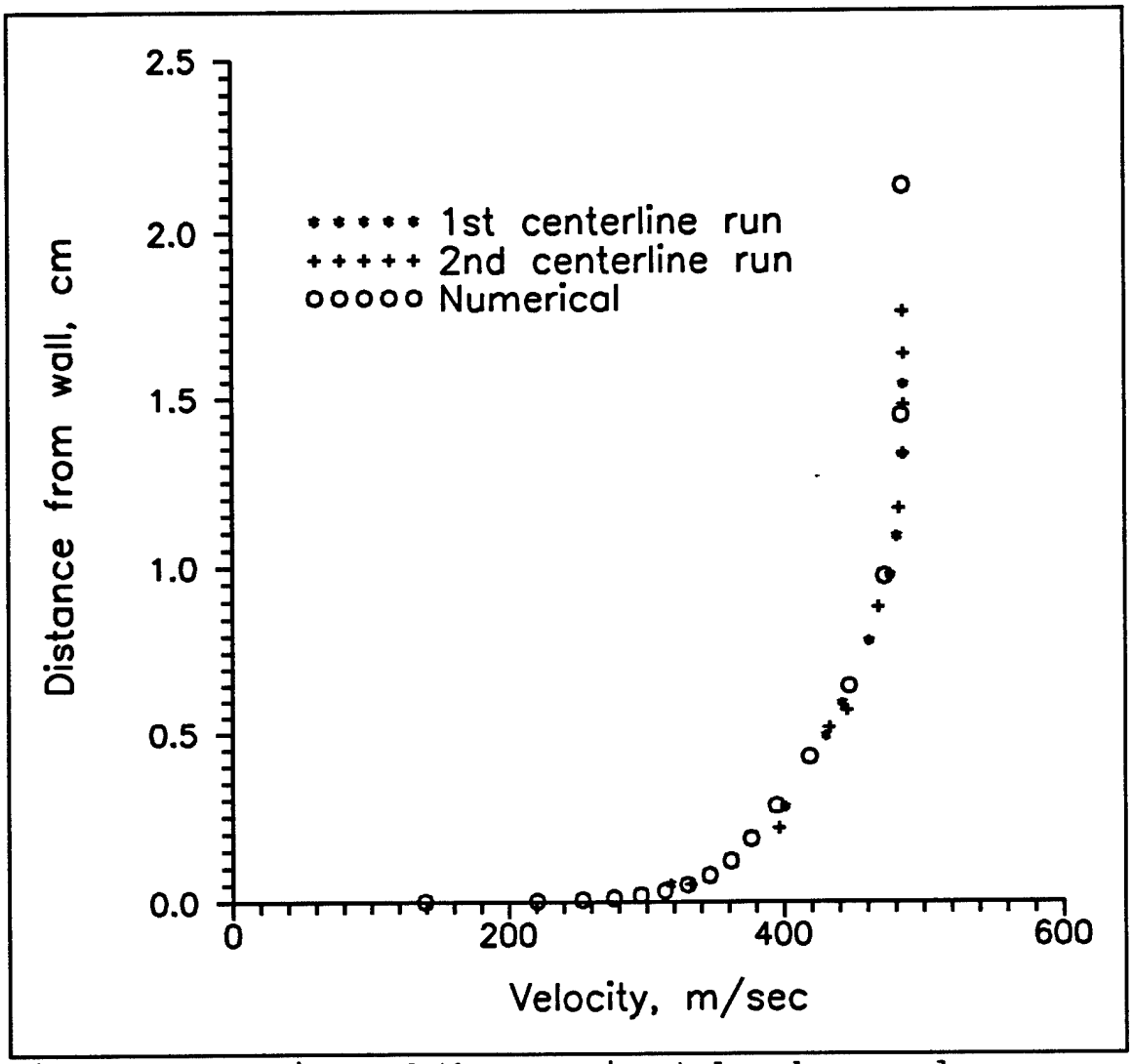

Figure 8 Comparison of the experimental and power law velocity profiles

Computational Issues

The results were obtained over a period of eighteen characteristic times (t_c). Data was sampled after $6t_c$ as suggested by Suhs. A sampling rate (for the surface pressure data) of $4.292x10^{-9}$ sec was employed. This corresponded to a maximum CFL of approximately 1. Run times for $18t_c$ were approximately 46 CPU hours on a Cray C-90 supercomputer.

The surface pressure was sampled each iteration at all points along the surface. A time average was then taken. Time averaged sound pressure levels ($\overline{SPLs}$) were computed at specific points on the surface via the equation

$$\overline{SPL} = 10\log_{10}\left(\frac{\overline{p'^2}}{q^2}\right)$$

where

$$\overline{p'^2} = \frac{1}{T}\int_{T_1}^{T_2}(p-\bar{p})^2\,dt$$

and the normalization variable, q, is the standard reference value from acoustics of $20\mu Pa$.

Field data was sampled at between 100 and 200 iteration rates because of the immense size of the resulting files. The results appear to indicate that this rate is sufficient to capture all significant solution changes.

Findings

The findings of this research are summarized in detail in references 24, 32 and 33. These papers and journal articles are included as appendices to this final report. Reference 32 appears both as a paper and a journal article therefore both are included.

Reference 24, "Observations on Using Experimental Data as Boundary Conditions for Computations," deals primarily with the specification of boundary conditions for the computation. As discussed earlier, specification of boundary conditions based on the experimental profile, the Crocco-Busemann relation and assumptions about the normal velocity is inadequate. As shown in figure 4 reference 24, a spurious wave forms in the extended solution of a flat plate unless all conditions are prescribed. The effect of this error on the computation of cavity flows is shown in figure 3 reference 24. In this figure results obtained with an experimentally determined inflow profile are compared to those obtained with an inflow profile that was obtained from a flat plate calculation with momentum thickness that matches the experiment. The inflow velocity profile for this comparison is shown in figure 2 of reference 24. These initial findings suggest that care should be taken when imposing boundary conditions based on experimental data. Because of these findings, a flat plate upstream calculation was performed to prescribe the inflow properties for all results performed in this research.

Reference 32, "A Comparison of Baldwin-Lomax Turbulence Models for 2-D Open Cavity Computations," details the comparison of the various turbulence models. Table 1 reference 32 lists the dominant frequencies recorded from these simulations at four points within the cavity. These results should be compared to the experimental value of 23 kHz obtained at the 2/3 point on the cavity floor, which matches the value computed from Rossiter's formula. It is clear that a range of solutions is obtained with these models, indicating that quite different unsteady results are obtained with the various modifications. However, it is unclear which result is best since there is no additional experimental or analytical evidence with which to compare. Surprisingly, the most "accurate" model is the LIA model. However, results for this model are not consistent throughout the cavity as would be suggested by Rossiter's formula. The multiple wall modification appears to provide the best comparison in that sense.

The results of the time average surface pressure comparisons are more mixed than the dominant frequency results. As described in reference 32 the results can be grouped according to the performance of the method on the back wall or the front wall and

floor. The best performers on the front wall and floor were SBL, ISU, LIA, REL, FL and FP, while the MW and SU models performed best on the aft wall. The latter comparison is probably the more important as structural damage will typically occur on the back wall based on the magnitude of the pressure fluctuations.

The most challenging comparison with experimental data was the time averaged sound pressure levels shown in figures 3, 4 and 5 of reference 32. These results are typically deceiving because they are presented on a log scale in the form of decibels. In these cases, apparently close results can be rather far off. The "best" result of this group was obtained by the REL model with the MW model a close second. Again, this comparison is not complete because no additional data points were obtained to confirm the apparent dip in SPL along the floor of the cavity. However, all of the models contain that qualitative feature. Maximum $\overline{SPL}$ was obtained for all models along the aft wall, where structural damage is typically expected. The magnitude of the $\overline{SPL}$ can be directly linked to the magnitude of the turbulent viscosity, as can the generic flow features to be discussed later. The highest values of the $\overline{SPL}$ were obtained with the laminar flow assumptions while the lowest value was obtained with the SBL model; the most dissipative scheme.

It is rather clear from the results shown in figures 6 and 7 of reference 32 that several peaks are present in the SPL vs frequency comparisons. This is markedly different than the experimental results which showed only a single peak. The meaning of this comparison is still unclear to the authors and merits further investigation.

Hinted at in the earlier results are the different flowfield behaviors observed with the various turbulence models. Figures 8 and 9 of reference 32 illustrate the differences in shear stress and flow field streamlines at the point of maximum aft wall pressure. The SBL is clearly the most dissipative scheme followed closely by the relaxation modification. However, the majority of the reduced viscosity flow fields are similar in appearance to the laminar flow cases. It is clearly difficult to make a determination as to the "best" approach due to the lack of experimental data, however, it is clear that a majority of the flows behave in a similar manner. The relatively good performance of the MW modification continues in this comparison as streamlines for this approach fall into that observed for the majority of methods.

The above results were further augmented by results from a combined approach utilized by Baysal. In this approach the FP, MW and REL models are combined. Results appear to match the best of the single model performances. A summary of

these results is found in reference 33, entitled "Supersonic Open Cavity Flow Physics Ascertained from Algebraic Turbulence Model Simulations." This paper is in draft form at this writing, however, the salient feature of this work is the comparison of the flow physics gleaned from the simulations viz. the oscillation cycle models of Rockwell and Naudascher, and Heller and Bliss. This portion of the work is ongoing and will be completed during the fall of 1996. However, the results shown in figure 1 of reference 33 indicate that the Rockwell and Naudascher vortex interaction explanation is viable. The streamlines clearly illustrate the shedding of a vortex and its subsequent interaction with the primary cavity vortex and the aft cavity edge. The shed vortex is observed more clearly in figure 3 reference 33, the vorticity contour series, as it sometimes enters the cavity and other times is torn apart by the aft corner. The vorticity contours further indicate that the primary vortex lies in the right "half" of the cavity and vorticity is shed left of the primary vortex from the cavity floor. It is this vorticity that tears the elongated shear layer which results in the shed vortex. Further study is needed to ascertain all of the important phenomena occurring in this flow.

Figure 2 of reference 33, the time series of the pressure contours, is also interesting from the standpoint of the oscillation cycles. This series is , of course, directly related to the Heller and Bliss cycle. However, it is not apparent from the contours that shock waves form within the cavity. It is quite clear that sharp external shocks are formed, but that the internal waves are compression waves and have not coalesced into shocks. Also apparent in this series is the fact that the internal waves are not planar but propagate at angles similar to that of the external waves. It is also not apparent that a wave "bounces" off the forward wall as suggested in Heller and Bliss' arguments. Again these issues will be fully examined by the fall of 1996.

To summarize, the findings of this research are

1. An experimental/computational approach can be successfully applied to study cavity flow physics.
2. Care must be taken when utilizing experimental data as boundary conditions for computations. In particular, unless complete specification of boundary conditions is possible, it is best to compute a similar upstream flow and match a parameter of the solution, such as momentum thickness.
3. Turbulent viscosity plays a critical role in cavity flow simulations. Specifically A) The dominant frequency of the cavity decreases as turbulent viscosity increases.

B) The magnitude of the time averaged sound pressure levels decrease as the turbulent viscosity increases.

C) Flow field features change dramatically with changes in turbulent viscosity, examples of this are turbulent viscous damping of both the primary and secondary vortices in the cavity.

4. Rockwell and Naudascher's vortex interaction description of the cavity oscillation cycle appears to be reasonable.
5. Heller and Bliss' pressure wave description of the cavity oscillation cycle appears to be deficient as it does not accurately reflect the flow physics observed in the simulations.
6. Rossiter's formula appears to match the experimental evidence (at zero degrees yaw) quite well and serves a valuable purpose when evaluating the accuracy of a numerical scheme.

Recommendations

The findings discussed above indicate that a considerable amount of information can be found by following a combined experimental/computational approach. However, more detailed information is needed for experimental validation of the computations including;

1. Additional surface pressure data for similar configurations.
2. Additional $\overline{SPL}$ data along the cavity surface.
3. Instantaneous flow visualization of the field.
4. Velocity field data at specific locations in the cavity. This data must be temporally correlated, perhaps to an event like the maximum aft wall pressure. This data would be useful for calibration of turbulence quantities provided a technique like conditional sampling is employed.
5. Determination of three dimensional effects on the cavity oscillation cycle. A recent paper by Sakamoto, Matsunaga, Fujii and Tamura[34] suggests that three dimensional effects are quite significant in cavity flows, contrary to statements by previous researchers.
6. Determination of the effects of yaw on open cavity oscillation physics.

This sort of evidence would complement and improve further computational investigations.

The results of the computations point to the inadequacy of the Reynolds averaged Navier-Stokes (RANS) approach. They indicate that none of the Baldwin-Lomax model modifications was acceptable for all performance goals. In fact, the unsteady accuracy metrics were perhaps best matched by the laminar flow calculations. This leads one to believe that a Direct Numerical Simulation (DNS) or a Large Eddy Simulation (LES) would be most appropriate for this type of flow field. In these approaches the small scale turbulent structures are adequately simulated by the computation with a minimum of modeling. It is apparent from the different turbulence model results that the small scales play an important role in defining the turbulent energy distribution.

It is important to note that the differences between the experimental and computational results cannot easily be attributed to three dimensional effects as many researchers often cite, because of the large aspect ratio of the cavity. Clearly some three dimensional effects are present, but not to the degree suggested by the

comparison. It is, of course, necessary to perform three dimensional calculations for a DNS or LES. Hence, it will be necessary to improve upon the basic performance of the numerical algorithm. In addition, turn-around time on many large Department of Defense supercomputers is often slow because of a large number of uses. Three dimensional simulations would therefore benefit from a code that could run in parallel, both from the inherent speedup efficiencies and the greater accessibility of the parallel machines. However, the performance at large Reynolds numbers of the DNS and LES approaches is limited by computational requirements. This further suggests a parallel algorithm approach since this will likely permit even greater computational performance in the near future.

Although a considerable amount can be learned about cavity flow physics mechanisms from RANS based simulations, lingering doubts will still exist until unsteady flow accuracy metrics can be validated. The best hope for learning these details in the near future is an LES based approach. The root cause of the cavity oscillation cycle could then be determined.

References

1. Roshko, A., "Some Measurements of Flow in a Rectangular Cutout," NACA Technical Note 3488, 1955.
2. McDearmon, R.W., "Investigation of the Flow in a Rectangular Cavity in a Flat Plate at a Mach Number of 3.55," NASA TN D-523, Sept. 1960.
3. Tracy, M.B., Plentovich, E.B., and Chu, J., "Measurements of Fluctuating Pressure in a Rectangular Cavity in Transonic Flow at High Reynolds Numbers," NASA TM 4363, June 1992.
4. Tracy, M.B., and Plentovich, E.B., "Characterization of Cavity Flow Fields Using Pressure Data Obtained in the Langley 0.3-Meter Transonic Cryogenic Tunnel," NASA TM 4436, March 1993.
5. Charwat, A.F., Roos, J.N., Dewey, C.F., and Hitz, J.A., "An Investigation of Separated Flows - Part I: The Pressure Field," *Journal of Aerospace Sciences,* Vol. 28, No. 6, pp 457-470. "Part II: Flow Separation in the Cavity and Heat Transfer," Vol. 28, No. 7, pp 513-527, 1961.
6. McGregor, O.W., and White, R.A., "Drag of Rectangular Cavities in Supersonic and Transonic Flow Including the Effect of Cavity Resonance," *AIAA Journal,* Vol. 8, No. 11, pp 1959-1964, Nov. 1970.
7. Catani, U., Bertin, J.J., DeAmicis, R., Masullo, S., and Bouslog, S.A., "Aerodynamics Characteristics for a Slender Missile with Wrap-Around Fins," *Journal of Spacecraft and Rockets*, Vol. 20, No. 2, March-April 1983.
8. Blair, A.B., Jr., and Stallings, R.L., Jr., "Supersonic Axial Force Characteristics of a Rectangular Box Cavity with Various Length-to-Depth Ratios in a Flat Plate," NASA TM-87659, 1986.
9. Hahn, M., "Experimental Investigation of Separated Flow over a Cavity at Hypersonic Speed," *AIAA Journal*, Vol. 7, No. 6, June 1969.
10. Nestler, D.E., Saydah, A.R., and Auxler, W.L., "Heat Transfer to Steps and Cavities in Hypersonic Turbulent Flow," *AIAA Journal*, Vol. 7, No. 7, July 1969.
11. White, R.A., "Some Results on the Heat Transfer within Resonant Cavities at Subsonic and Supersonic Mach Numbers," *ASME Journal of Basic Engineering*, Vol. 12, pp 537-542.
12. Nestler, D.E., "An Experimental Study of Hypersonic Cavity Flow," *Journal of Spacecraft and Rockets*, Vol. 19, No. 3, May-June 1982.
13. Rossiter, J.E., "Wind Tunnel Experiments on the Flow over Rectangular Cavities at Subsonic and Transonic Speeds," ARC R&M No. 3438, 1966.

14. Rockwell, D., and Knisley, C., "The Organized Nature of Flow Impingement Upon a Corner," *Journal of Fluid Mechanics*, Vol. 93, Part 3, 1970, pp 413-432.
15. Rockwell, D., and Naudascher, E., "Review-Self Sustaining Oscillations of Flow Past Cavities," *Journal of Fluids Engineering*, Vol. 100, June 1978, pp 152-165.
16. Heller, H., and Bliss, D., "Aerodynamically Induced Pressure Oscillations in Cavities: Physical Mechanisms and Suppression Concepts," AFFDL-TR-74-133, February 1975.
17. Zhang, X., and Edwards, J.A., "Computational Analysis of Unsteady Supersonic Cavity Flows Driven by Thick Shear Layers," *Aeronautical Journal*, pp 365-374, Nov. 1988.
18. Hankey, W.L., and Shang, J.S., "Analysis of Pressure Oscillations in an Open Cavity," *AIAA Journal*, Vol. 18, No. 8, August 1980, pp 892-898.
19. Tu, Y., "Unsteady Navier-Stokes Simulations of Supersonic Flow Over a Three-Dimensional Cavity," AIAA Paper 92-2632, June 1992.
20. Suhs, N.E., "Unsteady Computations for a Three-Dimensional Cavity With and Without an Acoustic Suppression Device," AIAA Paper 93-3402-CP, 1993.
21. Rizzetta, D.P., "Numerical Simulation of Supersonic Flow Over a Three-Dimensional Cavity," *AIAA Journal*, Vol. 26, No. 7, July 1988, pp 799-807.
22. Baysal, O., and Stallings, R.L., "Computational and Experimental Investigation of Cavity Flow Fields," *AIAA Journal*, Vol. 26, No. 1, January 1988, pp 6-7.
23. Simpson, L.B., and Whitfield, "Flux Difference Split Algorithm for Unsteady Thin-Layer Navier-Stokes Solution," *AIAA Journal*, Vol. 30, No. 4, pp 914-922, April 1992.
24. Orkwis, P.D., Tam, C.-J., and Disimile, P.J., "Observations on Using Experimental Data as Boundary Conditions for Computations," *AIAA Journal*, Vol. 33, No. 1, pp 176-178, January 1995.
25. Baldwin, B.S., and Lomax, H., "Thin Layer Approximation and Algebraic Model for Separated Turbulent Flows," AIAA Paper 78-257, January 1978.
26. Shang, J.S., and Hankey, W.L., Jr., "Numerical Solution for Supersonic Turbulent Flow Over a Compression Ramp," *AIAA Journal*, Vol. 13, No. 10, pp 1368-1374, October 1975.
27. Visbal, M., and Knight, D., "The Baldwin-Lomax Turbulent Model for Two-Dimensional Shock-Wave/Boundary-Layer Interactions," *AIAA Journal*, Vol. 22, No. 7, pp 921-928, July 1984.
28. Digenea, D., and Schiff, L.B., "Computation of Turbulent Supersonic Flows around Pointed Bodies Having Crossflow Separation," *Journal of*

Computational Physics, Vol. 66, No. 1, pp 173-196, September 1986.

29. Baysal, O., Private Communications, 1994.
30. Gorski, J.J., Ota, D.K., and Chakravarthy, S.R., "Calculation of Three Dimensional Cavity Flow Fields," AIAA Paper 87-0117, January 1987.
31. Baysal, O., Yen, G.-W., and Fouladi, K., "Navier-Stokes Computations of Cavity Aeroacoustics With Suppression Devices," Journal of Vibration and Acoustics, Vol. 116, No. 1, pp 105-112, January 1994.
32. Tam, C.-J., Orkwis, P.D., and Disimile, P.J., "A Comparison of Baldwin-Lomax Turbulence Models for 2-D Open Cavity Computations," *AIAA Journal*, April 1996; also "A Comparison of Several Standard Turbulence Models for 2-D Open Cavity Flow Field Computations," AIAA Paper 95-0361, January 1995.
33. Orkwis, P.D., Disimile, P.J., and Tam C.-J., "Supersonic Open Cavity Flow Physics Ascertained From Algebraic Turbulence Model Simulations," submitted in draft for presentation at the 34th AIAA Aerospace Sciences Meeting, Reno, NV, January 1996.
34. Sakamoto, K., Matsunaga, K., Fujii, K., and Tamura, Y., "Experimental Investigation of the Supersonic Internal Cavity Flows," AIAA Paper 95-2213, San Diego, CA, June 1995.

Appendix

- Orkwis, P.D., Tam, C.-J., and Disimile, P.J., "Observations on Using Experimental Data as Boundary Conditions for Computations," *AIAA Journal*, Vol. 33, No. 1, pp 176-178, January 1995.
- Tam, C.-J., Orkwis, P.D., and Disimile, P.J., "A Comparison of Baldwin-Lomax Turbulence Models for 2-D Open Cavity Computations," *AIAA Journal*, April 1996.
- Tam, C.-J., Orkwis, P.D., and Disimile, P.J., "A Comparison of Several Standard Turbulence Models for 2-D Open Cavity Flow Field Computations," AIAA Paper 95-0361, January 1995.
- Orkwis, P.D., Disimile, P.J., and Tam C.-J., "Supersonic Open Cavity Flow Physics Ascertained From Algebraic Turbulence Model Simulations," submitted in draft for presentation at the 34th AIAA Aerospace Sciences Meeting, Reno, NV, January 1996.

Observations on Using Experimental Data as Boundary Conditions for Computations

P. D. Orkwis, C.-J. Tam, P. J. Disimile

Reprinted from

AIAA Journal

Volume 33, Number 1, Pages 176–178

A publication of the
American Institute of Aeronautics and Astronautics, Inc.
370 L'Enfant Promenade, SW
Washington, DC 20024-2518

Observations on Using Experimental Data as Boundary Conditions for Computations

Paul D. Orkwis,* Chung-Jen Tam,† and
Peter J. Disimile‡
University of Cincinnati, Cincinnati, Ohio 45221

Introduction

MANY computational efforts have been undertaken to simulate phenomena that have been studied experimentally. Numerous examples of this are found in the recent work on open cavity flows by Hankey and Shang,[1] Rizzetta,[2] Baysal et al.,[3] and others. These computations attempted to match the conditions of an experiment by employing the same nondimensional flowfield parameters, such as Mach and Reynolds numbers, and identical geometries. However, without intimate knowledge of the experimental procedures and apparatus it is impossible to match all of the boundary conditions for these flowfields. This knowledge includes the data collection procedures, the construction of the model, the proximity of the wind-tunnel walls, and the conditions outside of the test section. Researchers typically either ignore these details or assume an idealized configuration. This Note describes the procedures employed by the authors to determine computational boundary conditions from an experimental supersonic open cavity flowfield study and the observations made during this process.

Observations

An experimental and computational research program[4] has been undertaken to study the flow physics of supersonic open cavity flowfields such as those encountered by stealthy fighter, attack, and bomber aircraft. This effort requires a synergistic approach to acquire valid field and surface data because neither experimental nor computational methodologies are capable of efficiently producing both. Acquired experimental data include time-averaged surface pressures, time histories of surface pressures, upstream boundary-layer streamwise velocities, and qualitative surface streaking using shear stress sensitive liquid crystals. Computational data include time histories of all field properties. These computational data can then be time averaged and compared with the surface data obtained

Presented as Paper 94-0589 at the AIAA 32nd Aerospace Sciences Meeting, Reno, NV, Jan. 10–13, 1994; received July 13, 1994; revision received Sept. 12, 1994; accepted for publication Sept. 30, 1994.

*Assistant Professor, Department of Aerospace Engineering and Engineering Mechanics. Member AIAA.

†Research Assistant. Member AIAA.

‡Associate Professor, Department of Aerospace Engineering and Engineering Mechanics. Member AIAA.

in the experiments to assess the accuracy of the computations and to validate the turbulence modeling assumptions. This approach then produces valid qualitative and quantitative field and surface property information that can be used to uncover the dynamic mechanisms that drive open cavity flowfields.

Two-dimensional flows were simulated by employing a cavity with a width-to-length ratio (W/L) of approximately 12 and a length-to-depth ratio (L/D) of 2, as shown in Fig. 1. The wind-tunnel freestream conditions for these tests were Mach number $M = 2$ and unit Reynolds number $Re/L = 37.7 \times 10^6$/m.

It was initially assumed that the experimental data would be ideal for the purpose of determining valid upstream boundary conditions for the cavity computations. Therefore, pitot pressure surveys were conducted (several times to assure repeatability) 1.94 cm upstream of the cavity separation lip to determine the upstream velocity profile shown in Fig. 2. These data were then fitted to a power law profile with an exponent of 8.4, which allowed velocities to be found at all computational grid points. A temperature profile was then found by employing the turbulent Crocco-Busemann relation

$$T = T_w + (T_{aw} - T_w)\frac{u}{U_\infty} - r\frac{u^2}{2C_p} \qquad (1)$$

with the experimentally determined wall temperature of 239 K. It should be noted that in Eq. (1) w corresponds to wall conditions, aw to adiabatic wall conditions, and r to the recovery factor, i.e., $P_r^{\frac{1}{3}}$, where P_r is the Prandtl number. The remaining variables, density and total energy, were then found by assuming a perfect gas and zero normal velocity.

However, the zero normal velocity assumption proved to be detrimental to the computational solution, as can be seen in the computed time-averaged cavity surface pressures shown in Fig. 3 for two different inflow conditions. In case A the power law profile discussed earlier was used as the inflow velocity distribution, and in case B a computationally generated flat plate solution was employed that matched the experimental momentum thickness (shown in Fig. 2). Both sets of results were obtained using the standard Baldwin-Lomax turbulence model and a computational grid with a minimum y^+ of 44. Results from five cavity characteristic times, defined as L/U_∞ (L is the cavity length) were used to obtain the averages. The results compared quite well with the experimental data when the computational inflow condition was used, but the results

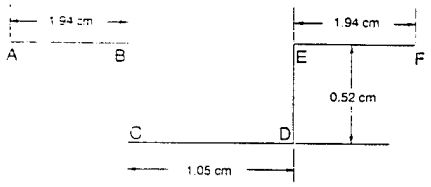

Fig. 1 Two-dimensional cavity schematic.

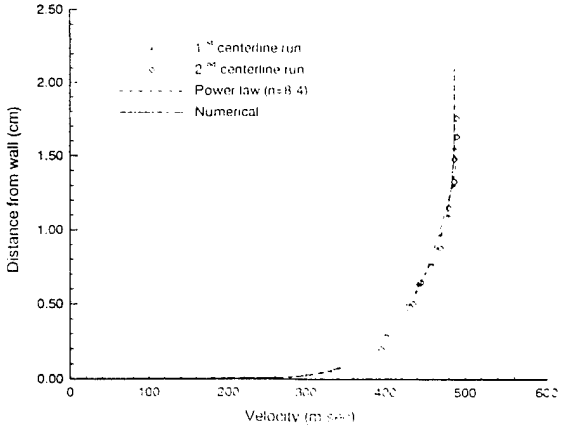

Fig. 2 Comparison of experimental and computational velocity

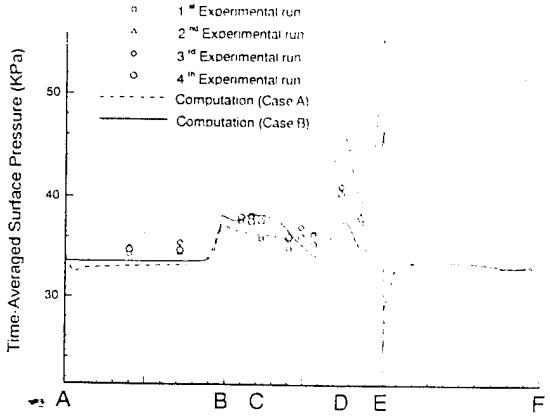

Fig. 3 Comparison of experimental and computational surface pressures.

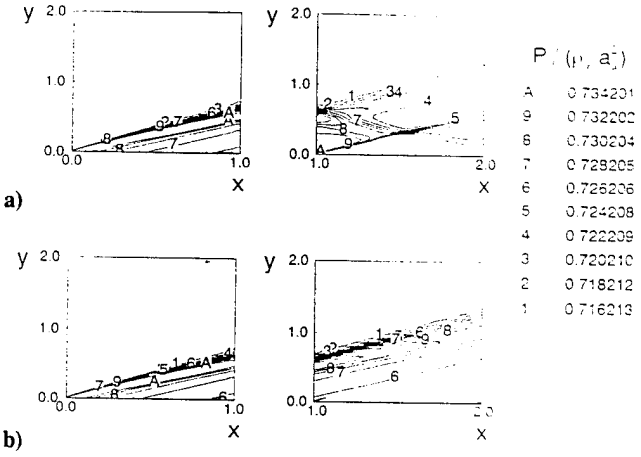

Fig. 4 Pressure contours of consecutive flat plate calculations: a) zero normal velocity and b) actual velocity.

differed by as much as 11% when the experimental profile with zero normal velocity was employed.

The differences in the results were caused by the assumption of zero normal velocity. This was proven by a numerical study that produced the pressure contour results shown in Fig. 4, in which upstream boundary conditions derived from an initial flat plate solution were used to extend the flat plate solution further downstream. The flow properties from the next to last grid line of the initial flat plate were used as the upstream boundary condition for the flat plate extension. Case A employed a profile with zero normal velocity and case B used the full velocity profile. The left contours for both cases are from the same initial flat plate solution. The contours clearly illustrate the formation of spurious shock and expansion waves as a result of the $v = 0$ assumption. Similar contours are produced for the other solution variables and are not shown.

It should be noted that the previous configuration is not the same as that used in the cavity flow computations. In that case a much longer plate was required to match the experimental momentum thickness; consequently, the bow shock wave propagated out of the solution domain. The shorter plate was employed in the previous computation because it provides a much clearer example of the errors inherent in neglecting small velocity components. In addition, the initial drop in surface pressure of the cavity model (see Fig. 3) clearly demonstrates similar trends. These discrepancies might be lessened if the point of boundary condition application was moved further upstream, since the flow would have a greater distance to adjust to the erroneous velocity specification. The results show that care must be taken to insure complete specification of boundary conditions if experimental data are to be employed.

Summary

This effort has shown that a complete description of the flowfield

computational simulation that is to match experimental data. Inclusion of the experimental normal velocity was shown to be vital for the derivation of correct computational boundary conditions. Streamwise velocity profiles determined from pitot probe measurements were found to be insufficient for this purpose; hence, techniques capable of determining both streamwise and normal velocity must be employed.

Acknowledgments

The authors wish to thank Dr. Leonidas Sakell and the Air Force Office of Scientific Research for their generous support through Grant F49620-93-1-0081. This work was supported in part by a grant of HPC time from the Department of Defence HPC Shared Resource Center, U.S. Army Corps of Engineers—Waterways Experiment Station C916/16512 Supercomputer.

References

[1]Hankey, W. L., and Shang, J. S., "Analysis of Pressure Oscillations in an Open Cavity," *AIAA Journal*, Vol. 18, No. 8, 1980, pp. 892–898.

[2]Rizzetta, D. P., "Numerical Simulation of Supersonic Flows over a Three-Dimensional Cavity," *AIAA Journal*, Vol. 26, No. 7, 1988, pp. 799–807.

[3]Baysal, O., Fouladi, K., Leung, R. W., and Sheftic, J. S., "Interference Flows Past Cylinder-Fin-Sting-Cavity Assemblies," *Journal of Aircraft*, Vol. 29, No. 2, 1992, pp. 194–202.

[4]Dusing, D. W., Fox, C. W., Tam, C.-J., Orkwis, P. D., and Disimile, P. J., "An Experimental and Computational Study of Unsteady Supersonic 2-D Open Cavity Flow Physics," AIAA Paper 94-0589, Jan. 1994.

Observations on Using Experimental Data as Boundary Conditions for Computations

P. D. Orkwis, C.-J. Tam, P. J. Disimile

Reprinted from

AIAA Journal

Volume 33, Number 6, Page 1167

AIAA

A publication of the
American Institute of Aeronautics and Astronautics, Inc.
370 L'Enfant Promenade, SW
Washington, DC 20024-2518

Errata

Observations on Using Experimental Data as Boundary Conditions for Computations

Paul D. Orkwis, Chung-Jen Tam, and Peter J. Disimile
University of Cincinnati, Cincinnati, Ohio 45221

[AIAA Journal, 33(1), pp. 176–178 (1995)]

DURING production of this paper, a measurement was incorrectly stated. AIAA regrets the error.

Page 177

In the paragraph that begins "However, the zero normal velocity . . . ," the third sentence should read as follows:

Both sets of results were obtained using the standard Baldwin–Lomax turbulence model and a computational grid with a minimum y^+ of 4.4.

AIAA 95-0361

A Comparison of Several Standard Turbulence Models for 2-D Open Cavity Flow Field Computations

Chung-Jen Tam
Paul D. Orkwis
and
Peter J. Disimile
University of Cincinnati
Cincinnati, OH

REVISED
FEB. 9, 1995

33rd Aerospace Sciences Meeting and Exhibit
January 9-12, 1995 / Reno, NV

A COMPARISON OF SEVERAL STANDARD TURBULENCE MODELS FOR 2-D OPEN CAVITY FLOW FIELD COMPUTATIONS

by
Chung-Jen Tam *
Paul D. Orkwis †
and
Peter J. Disimile ‡
University of Cincinnati
Cincinnati, Ohio

ABSTRACT

This paper presents a comparison between results obtained using several modifications of the Baldwin-Lomax algebraic turbulence model for the unsteady flow field about a supersonic 2-D open cavity. The tested modifications include the upstream relaxation, first peak, multiple-wall, Suhs' and inverse Suhs' approaches and laminar flow in and above the cavity. Results from these methods are compared to experimental data. Time averaged surface pressures and sound pressure levels, surface pressure time history frequency content at several locations, streamlines and shear stress contours were compared. None of the tested models were clearly superior, although the multiple-wall modification was found to be adequate in all tests. A distinct relationship between turbulent viscosity and quality results was also observed. the standard Baldwin-Lomax model consistently under performed on all tests.

INTRODUCTION

The presence of a cavity in a surface bounding a fluid flow can cause large pressure, velocity, and density fluctuations in its vicinity as well as strong propagating acoustic waves. In addition, the drag on the surface can be altered and structural failure due to resonance can occur. Such flows are of interest in many different areas of engineering. Landing-gear wells and bomb-bays on aircraft are common examples of cavities in which reduction of pressure fluctuations, noise generation, and sonic fatigue are of prime concern.

Supersonic cavity flow fields contain a mixture of unsteady flow regimes which may include oscillating shear layers that shed vortices in coherent patterns, unsteady weak shock or pressure waves, and vortices in the transverse and streamwise directions which reside within the cavity. The shear layer location depends upon conditions both inside and outside of the cavity, and in turn affects the internal and external flow fields near the cavity. This interaction is the result of an extremely complicated flow pattern which appears to depend upon the shape of the cavity (allowing it to be classified as either open, closed or transitioning [1,2]), the Mach number, and the Reynolds number.

Numerous prior investigations [3,4,5,6] have been conducted in order to gain insight into the underlying physical behavior of cavity flows. While most of these have been experimental, simplified analytic analyses and empirical techniques, including those of Rossiter [7], have made it possible to predict some of the features of the observed phenomena. In addition, numerical solutions of the Navier-Stokes equations have provided detailed flow field descriptions that were not obtainable by experimental methods.

However, a persistent problem with the numerical simulation of cavity flow is the choice of an appropriate turbulence model. Hankey and Shang [5] analyzed pressure oscillations in open cavities by solving the unsteady Navier-Stokes equations using the Cebeci-Smith [8] turbulence model with the relaxation modification [9]. Gorski et al. [10] used the Baldwin-Lomax turbulence model with a wall modification as well as a high Reynolds number κ-ϵ turbulence model with a near-wall modification. Suhs [11] applied the standard Baldwin-Lomax model for the flat plate and bottom wall of the cavity, and assumed laminar flow in the shear layer region above the cavity. Rizzetta [12] and Tu [13] used the Baldwin-Lomax model with the relaxation model for 3-D supersonic open cavity flows. Ramakrishnan et

---

* Student Member AIAA, Graduate Assistant
† Member AIAA, Assistant Professor of Aerospace Engineering & Engineering Mechanics
‡ Member AIAA, Associate Professor of Aerospace Engineering & Engineering Mechanics

al. [14] investigated hypersonic closed cavity flow using both a Baldwin-Lomax and a one-equation turbulence model. Baysal et al. [15] have researched supersonic open cavity flows using the Baldwin-Lomax turbulence model and a combination of the relaxation modification, the first peak modification, and the multiple-wall modification. Atwood [16] used the Baldwin-Lomax turbulence model in computations of transonic cavity flows for the study of the Stratospheric Observatory For Infrared Astronomy (SOFIA). Shih [17] developed a numerical scheme which coupled the κ-ϵ turbulence model equations with the Navier-Stokes equations for a 2-D supersonic open cavity flow.

Although many turbulence model modifications for cavity flow fields have been proposed, little evidence has been offered as to the suitability of a particular choice. Time averaged surface pressure data appear to agree quite well for all models, but apparently different flow field behavior has been reported. An understanding of which model computes accurately the surface properties while at the same time simulating the field data is still required.

This paper presents the numerical results of a 2-D open cavity flow field study that employed the double thin-layer Navier-Stokes equations and various versions of the Baldwin-Lomax algebraic turbulence model. The results are compared to the experimental data of Disimile and Orkwis [18]. These results represent the first step in an effort designed to determine appropriate turbulence models for unsteady field computations. A parallel experimental effort is being performed to gather valid unsteady turbulence quantity data for this work.

The following sections discuss the governing equations, the numerical scheme, the turbulence models, the results and a summary.

GOVERNING EQUATIONS

The unsteady Reynolds averaged double thin-layer Navier-Stokes (DTLNS) equations were discretely solved in this work. The DTLNS equations retain the viscous terms in both the x and y directions as opposed to the thin-layer Navier-Stokes (TLNS) equations which retain term only in the y direction. The TLNS equations have been described by many researchers [19,20], and as such they will not be included here. The DTLNS equations are solved using the implicit approximate factorization of Simpson and Whitfield [20].

NUMERICAL METHOD

The original numerical method used by Simpson and Whitfield employed an implicit upwind finite volume scheme to solve the three-dimensional TLNS equations. The modified code for the cavity computations employs the DTLNS equations. The residuals are formed by using Roe's flux-difference splitting and achieve third order accuracy in the spatial direction using the techniques developed by Osher and Chakravarthy. The Van Albada limiter is used to damp nonphysical oscillations near discontinuities, while approximate factorizations are used to solve the system of equations.

The linearized implicit form of the discrete governing equations can be split into flux vectors with either non-negative (indicated by a plus superscript) or non-positive eigenvalues (indicated by a negative superscript). Appropriate upwind differencing gives the approximate implicit scheme

$$(I + \Delta\tau\nabla_\xi A^+ + \Delta\tau\nabla_\eta B^+ + \Delta\tau\nabla_\zeta C^+ + \Delta\tau\Delta_\xi A^- + \Delta\tau\Delta_\eta B^- + \Delta\tau\Delta_\zeta C^-)\Delta Q^n = -\Delta\tau R^n \quad (1)$$

where

$$R^n = -\Delta\tau\left(\frac{\partial F^n}{\partial\xi} + \frac{\partial G^n}{\partial\eta} + \frac{\partial H^n}{\partial\zeta} + \frac{\partial S_v^n}{\partial\eta}\right) \quad (2)$$

Equation 1 can then be written as an approximate system of the form

$$(I + \Delta\tau\nabla_\xi A^+ + \Delta\tau\nabla_\eta B^+ + \Delta\tau\nabla_\zeta C^+) * (I + \Delta\tau\Delta_\xi A^- + \Delta\tau\Delta_\eta B^- + \Delta\tau\Delta_\zeta C^-)\Delta Q^n = -\Delta\tau R^n \quad (3)$$

The flux Jacobians in the above equation are then obtained from the Steger-Warming flux vector splitting, and the residual vector, R^n, from Roe's flux difference splitting.

The solution to equation 3 is found in the following manner

$$(I + \Delta\tau\nabla_\xi A^+ + \Delta\tau\nabla_\eta B^+ + \Delta\tau\nabla_\zeta C^+)X^1 = -\Delta\tau R^n \quad (4)$$

$$(I + \Delta\tau\Delta_\xi A^- + \Delta\tau\Delta_\eta B^- + \Delta\tau\Delta_\zeta C^-)X^2 = X^1 \quad (5)$$

$$\Delta Q^n = X^2 \quad (6)$$

Equations 4, 5 and 6 require the solution of two linear systems. The first equation is solved in a forward pass, resulting in a lower block bi-diagonal system, and the second term is solved by a backward pass resulting in an upper block bi-diagonal system. The solution of the equations gives the desired solution vector, $\Delta^n Q$, from which the dependent variable vector at time level $n+1$ can be obtained

$$\Delta Q^{n+1} = Q^n + \Delta^n Q \quad (7)$$

The resulting numerical method can be run second order accurate in time by employing a Newton subiteration procedure as discussed below.

UNSTEADY SOLUTIONS

A Newton-like subiteration procedure is performed at each iteration for the unsteady calculations. This procedure can be thought of as a pseudotime iteration which recovers full temporal accuracy after psuedotime convergence. Acceptable convergence is typically obtained with four subiterations and frozen Jacobians, as shown by Simpson and Whitfield [20]. The implementation of the subiterations into the algorithm can be easily described by considering the following temporally first order algorithm

$$(I + \Delta\tau\nabla_\xi A^+ + \Delta\tau\nabla_\eta B^+ + \Delta\tau\nabla_\zeta C^+) * (\Delta\tau\delta_\xi A^- + \Delta\tau\delta_\eta B^- + \Delta\tau\delta_\zeta C^-)\Delta Q^p = RHS^p \quad (8)$$

where

$$RHS^p = -\Delta\tau\left[\frac{Q^p - Q^n}{\Delta\tau} + \left(\frac{\partial F^p}{\partial\xi} + \frac{\partial G^p}{\partial\eta} + \frac{\partial H^p}{\partial\zeta}\right)\right] \quad (9)$$

ΔQ^p is defined as

$$\Delta Q^p = Q^p - Q^{p-1} \quad (10)$$

and p is a subiteration counter. At convergence $Q^p \rightarrow Q^{n+1}$, and the viscous terms are no longer time lagged.

Second order temporal accuracy can be achieved by employing data at additional time levels and appropriate temporal differences.

TURBULENCE MODELS

The present computations were performed with the Baldwin-Lomax [21] turbulence model and several modifications including the upstream relaxation, first peak, multiple-wall, Suhs', and inverse Suhs' approximations. Laminar flow in and above the cavity and laminar flow everywhere in the computational space were also attempted.

The Baldwin-Lomax model is a two-layer algebraic eddy viscosity model in which μ_t is given by

$$\mu_t = \begin{cases} (\mu_t)_{inner} & y \le y_{crossover} \\ (\mu_t)_{outer} & y_{crossover} \le y \end{cases} \quad (11)$$

where y is the normal distance from the wall and $y_{crossover}$ is the smallest y value at which values from the inner and outer formulas are equal.

The Prandtl-Van Driest formulation of the eddy viscosity is used in the inner region

$$(\mu_t)_{inner} = \rho\ell^2|\omega| \quad (12)$$

where

$$\ell = ky\left[1 - \exp\left(-\frac{y^+}{A^+}\right)\right] \quad (13)$$

and $|\omega|$ is the magnitude of the vorticity

$$|\omega| = \sqrt{\left(\frac{\partial u}{\partial y} - \frac{\partial v}{\partial x}\right)^2 + \left(\frac{\partial v}{\partial z} - \frac{\partial w}{\partial y}\right)^2 + \left(\frac{\partial w}{\partial x} - \frac{\partial u}{\partial z}\right)^2} \quad (14)$$

and

$$y^+ = \frac{\rho_w u_\tau y}{\mu_w} = \frac{\sqrt{\rho_w \tau_w}\, y}{\mu_w} \quad (15)$$

The Baldwin-Lomax model uses the Clauser formulation for the outer region of the eddy viscosity

$$(\mu_t)_{outer} = KC_{CP}\rho F_{WAKE}F_{KLEB}(y) \quad (16)$$

where K is the Clauser constant, C_{CP} is an additional constant, and

$$F_{WAKE} = \min\begin{cases} y_{MAX}F_{MAX} \\ C_{WK}y_{MAX}u_{DIF}^2/F_{MAX} \end{cases} \quad (17)$$

The quantities y_{MAX} and F_{MAX} are determined from the function

$$F(y) = y|\omega|\left[1 - \exp\left(-\frac{y^+}{A^+}\right)\right] \quad (18)$$

The quantity F_{MAX} is the maximum value of F(y) that occurs in a profile and y_{MAX} is the value of y at which it occurs.

The function $F_{KLEB}(y)$ is the Klebanoff intermittency factor given by

$$F_{KLEB}(y) = \left[1 + 5.5\left(\frac{C_{KLEB}y}{y_{MAX}}\right)^6\right]^{-1} \quad (19)$$

and

$$U_{DIF} = (\sqrt{u^2 + v^2 + w^2})_{MAX} - (\sqrt{u^2 + v^2 + w^2})_{MIN} \quad (20)$$

The second term in U_{DIF} is taken to be zero. The values of the constants are:

$$A^+ = 26,\ C_{CP} = 1.6,\ C_{KLEB} = 0.3,$$

$$C_{WK} = 0.25,\ k = 0.4,\ K = 0.0168$$

This algebraic eddy viscosity model is simple and practical; consequently, it is used extensively. However, there are several limitations to this type of model. For one, the reference lengths are different for various types of flows, such as wall boundary layers, jets, and wakes. In the case of cavity flow, the reference length for the flat plate region is different from that within the cavity. Secondly, the model evaluates the turbulent viscosity based only on local flow variables without regard to surrounding conditions. In the cavity, the standard Baldwin-Lomax turbulence model produces a discontinuous eddy viscosity due to the abrupt change in the reference length as compared to the flat plate. Therefore some model modifications have arisen in the study of open-cavity flow fields. Many researchers have employed these models in similar computations but no definitive comparison has been performed to determine which performs best.

RELAXATION MODIFICATION

The abrupt change in the eddy viscosity coefficient from the boundary layer to the free shear layer is eliminated by using the relaxation modification. This technique was first applied by Shang and Hankey [22] in the study of a supersonic compression ramp. In this scheme, the original Baldwin-Lomax model is used to compute the initial values of the eddy viscosity, and then the actual values are computed from

$$\mu_t = \mu_{tu} + (\mu_{ts} - \mu_{tu})\left[1 - \exp\left(-\frac{x}{10\delta}\right)\right] \quad (21)$$

where, μ_{ts} is the unaltered Baldwin-Lomax turbulent viscosity, μ_{tu} is the upstream turbulent viscosity above the cavity lip, δ the instantaneous boundary layer thickness at the upstream corner, and x is the streamwise distance from the corner. This modification has been shown to work well in numerical calculations of compression corner flows with separation by Visbal and Knight [23]. It produces a weighted average of the local eddy viscosity with the upstream value, thereby producing a more continuous variation of μ_t.

FIRST PEAK MODIFICATION

Another major difficulty encountered in applying the Baldwin-Lomax turbulence model is the evaluation of the reference length, y_{MAX}, and in turn the determination of $(\mu_t)_{outer}$, for the boundary layer profiles within the cavity. In recirculation regions, the function F(y) has multiple peaks. A larger peak caused by the overlying vortex structure can be found in addition to the peak due to the attached boundary layer. Choice of the second / larger peak for F_{MAX} results in a $(\mu_t)_{outer}$ value that is larger than that obtained with the first peak. The first peak modification forces F_{MAX} to be the value associated with the first maxima. Its general effect is to reduce the overall eddy viscosity throughout most of the shear layer. This technique had been applied by Degani et al. [24] and Praharaj et al. [25] in the supersonic flow around pointed bodies and by Baysal [26] for supersonic open cavity flows.

MULTIPLE-WALL MODIFICATION

In this modification the effects of multiple-walls are included for points within the cavity as per Gorski et al. [10] and Baysal et al. [15]. This is accomplished by using the inverse averaging method to compute μ_t values that are influenced by two different walls. The eddy viscosity is then calculated using the formula

$$\mu_t = \frac{\frac{\mu_{t_{w1}}}{y_1^+} + \frac{\mu_{t_{w2}}}{y_2^+}}{\sqrt{\left(\frac{1}{y_1^+}\right)^2 + \left(\frac{1}{y_2^+}\right)^2}} \quad (22)$$

where μ_{tw1}, is the turbulent viscosity obtained by applying the Baldwin-Lomax model normal to wall 1 and μ_{tw2} is that obtained from wall 2. This formulation allows the wall with the lower y^+ value (usually the closest wall) to be relatively more important that the neighboring wall. This technique is applied in the cavity using the two vertical walls and the floor to compute the eddy viscosity. (Again the general effect of this modification is a lower eddy viscosity in regions near the aft vertical walls of the cavity.)

SUHS' MODIFICATION

Suhs [11] investigated 3-D open cavities using the Baldwin-Lomax turbulence model. The model was applied on the flat plate and the bottom wall of the cavity, but no turbulence model was used in the shear layer region above the cavity.

INVERSE SUHS' MODIFICATION

Since the Suhs model does not at first glance appear physically realistic, it was decided to test the reverse

idea. That is, the Baldwin-Lomax turbulence model was applied for the flat plates and above the cavity, but no turbulence model is used in the cavity.

LAMINAR FLOW IN AND ABOVE THE CAVITY

To further extend the reasoning behind the Suhs model, laminar flow in and above the cavity was tested. That is, no turbulence model was implemented in and above the cavity, while the standard Baldwin-Lomax turbulence model was used for the flat plate regions.

FULLY LAMINAR

Lastly, to test the limits of allowable turbulent viscosity, laminar flow everywhere in the flow field was also tested.

INITIAL/BOUNDARY CONDITIONS

Boundary conditions were obtained from a flat plate computation that simulated the experimental wind tunnel wall boundary layer momentum thickness as discussed by Orkwis et al. [27]. The test parameters for the supersonic wind tunnel were $M_\infty = 2$, $Re_\theta = 3.69 \times 10^4$ with a boundary layer momentum thickness of 0.979 mm.

The flow above the cavity was initialized using the conserved variables from the last column of the flat plate solution. The flow within the cavity was obtained by density and pressure everywhere specified equal to the flat plate wall values and setting $\rho u = 0.5$, $\rho v = \rho w = 0.0$. The total energy was then defined from these quantities.

RESULTS AND DISCUSSION

The results are grouped into surface and field properties. The surface properties include both time averages and time histories of pressure and sound pressure levels. Field properties are presented in the form of streamlines and shear stress contours.

The grids for this study had 66x55, 66x120 and 66x55 number of cells for the three blocks. A total of 15,180 grid points were employed. The block cuts were prescribed to eliminate block boundary error effects along the shear layer. Points were clustered along all walls using the function

$$x_p = \frac{e^{-k\left(\frac{j}{N}-1\right)} - 1}{e^k - 1} \qquad (23)$$

where j is the point index and N the total number of points. This grid was chosen based on the results of a grid resolution study, the results of previous researchers, and available computational resources. Solutions were computed on grids with half and double point densities in both the x and y directions to test the suitability of the chosen grids. The results from the finer grids were only marginally different.

The results were obtained over a period of 18 characteristic times (t_c). Data was sampled after 6 t_c as per the suggestion of Suhs [11]. A sampling rate 4.292×10^{-9} sec was employed. Run times for 18 t_c were approximately 46 hours on a Cray C-90 supercomputer. A total of 8 runs are reported, which required approximately 368 CPU hours.

SURFACE PROPERTIES

Surface properties are typically used for comparisons with experimental data because experiments are capable of generating only limited amounts of field data in reasonable times. These data allow one to compute drag and heat transfer effects, but only allow limited comparisons with flow field features. Hence, this sort of data must be considered a starting point for turbulence model comparison purposes.

Pressure

Figures 2a, b and c contain comparison of the time averaged surface pressures obtained from the experiment and the tested turbulence models. In general, cavity pressures were not much greater than the freestream values, approximately 15%. This is similar to the results reported by Rizzetta. The highest pressure was found at the aft wall/floor intersection.

The general results can be grouped according to their performance on the forward/bottom walls and the aft wall. The best performers for one case were the worst performers for the other. This points to the fact that none of these models provided adequate surface pressure results over the entire cavity.

The best models for the front and bottom walls were the standard Baldwin-Lomax (SBL), inverse Suhs' (ISU), fully laminar (FL), laminar in and above the cavity (LIA), relaxation (REL), and first peak (FP). The worst performers over this range were the Suhs' (SU) and multiple-wall (MW) models. Surprisingly, this situation was completely reversed for the aft wall, with SU and MW performing best and SBL, ISU, LIA, REL, FL and FP models performing poorly. Note that although the MW and SU models both perform well on the aft wall, the SU model always performed better. It is also important to note that the aft wall is the most important from a standpoint of structural integrity because it endures the highest loads.

In general, it is surprising that the results do not differ

greatly between models. In fact, even the FL computation performed reasonably well on the aft wall. A trend that developed with these results can be observed by considering the general shape of the figures. Note that the SBL model varies in the smoothest fashion, whereas the FL model contains the most oscillations. This is a consequence of the turbulent viscosity levels and will be discussed in greater detail in a later section.

Sound Pressure Levels

The time histories of the surface pressures were recorded and used to form time averaged sound pressure levels ($\overline{SPL}$) at twenty points within the cavity. Five points each were used on the forward and aft walls, while ten points were recorded along the bottom wall. The time history was used to compute the $\overline{SPL}$ via the equation

$$\overline{SPL} = 10\log_{10}\left(\frac{\overline{p^2}}{q^2}\right) \tag{24}$$

where

$$\overline{p^2} = \frac{1}{T}\int_{T_1}^{T_2}(p-\bar{p})^2 dt \tag{25}$$

The time average of the pressure fluctuations squared is normalized by q, the standard reference value for acoustics, 20 μPa.

The same trend emerges for each wall as shown in Figures 3-5. The results are similar to those presented by Rizzetta. It should be noted that these plots use a decibel scale which is logarithmic. Hence, deceptively small differences can be quite large. The data show that $\overline{SPL}$ varies greatly with model. Along the forward wall values ranged from 158db to 172db, along the floor it varies from 152db to 180db, and along the aft wall from 160db to 180db. Along the front wall, the $\overline{SPL}$ was greatest at the cavity lip. The SBL model produced the lowest values of $\overline{SPL}$ while values from the FL case were typically near the largest. However, some of the turbulence model results produced $\overline{SPL}$ values greater than FL. This perhaps suggests that turbulent viscosity is not the only parameter affecting $\overline{SPL}$.

The $\overline{SPL}$ along the cavity floor generally increased in the downstream direction, with the exception of a pronounced dip at the approximate center of the cavity floor. The experimental data show that the REL model compared quite well at this point although the MW model was also close as shown in Figure 4a. All of the other approaches were at least 3db from the experimental data, with the SBL giving the maximum difference of 8db. Again, the LIA and FP produced greater $\overline{SPL}$s than FL. This could perhaps be explained by the differences in incoming boundary layer caused by using the FL assumption for the upstream flat plate.

Recall that the highest time averaged pressure occurred along the aft wall. This is reflected in the $\overline{SPL}$s as well, with the greatest values occurring in the lower right corner in Figure 5a-b. The same general trends occurred as were obtained with the other walls, including the SBL producing by far the lowest values of $\overline{SPL}$.

The surface property results provide clues as to the behavior of the respective turbulence models. It can be conjectured that turbulent viscosity plays an significant role in both the $\bar{p}$ and $\overline{SPL}$ results. Smoother $\bar{p}$ and lower $\overline{SPL}$ values were obtained as the viscous dissipation increased. This general trend is reflected in later results as well.

TIME HISTORIES

The time averaged properties discussed above contain no information about instantaneous events in the cavity. To learn more about these items one must analyze time histories of surface properties and explore the associated frequency spectra. To that end, a Fast Fourier Transform (FFT) was used to decompose the pressure signal. The resulting FFT is a plot of the pressure perturbation squared versus frequency. This can be transformed to SPL at a specific location versus frequency using equations 24 and 25. FFTs of the SPL and pressure perturbations were computed at the center of each cavity wall and at the two thirds point on the cavity floor. The latter allow comparison with the available experimental data.

Figure 6 shows the SPL and pressure perturbation FFTs at the x/L = 2/3 point for the relaxation model. The region from 0 to 100 kHz was enlarged to illustrate the dominant peak in the pressure perturbation plot. This information becomes blurred by the conversion to SPL because of the decibel scale. The FFTs for all models show similar overall trends, however, the dominant frequencies and respective magnitudes are different.

It is expected that the dominant cavity frequency will match that described by the empirical correlation of

Rossiter [7], which can be found from the equation

$$f = \frac{U}{L}\frac{(m-\gamma)}{(1/K + M)} \quad , \quad m = 1,2,3,... \qquad (26)$$

where γ = 0.25 and K = 0.66 are constants, U is the freestream velocity, L the cavity length, M the freestream Mach number and m the stages. This formula gives $f_{m=1}$ = 9916 Hz, $f_{m=2}$ = 23,138 HZ, and $f_{m=3}$ = 36,360 Hz. Rossiter notes that the dominant peak is one of these values, although not necessarily the first.

Figures 7a and b show the results of the SPL FFTs conducted at x/L = 2/3. Figures of this type were then used to determine the dominant frequencies. Results obtained at 4 cavity locations are summarized in table 1.

It is rather clear from the results that viscosity reduces considerably the dominant frequency, although it is unclear how the specific modifications affect the results within the cavity. As noted earlier, the SBL produced the greatest turbulent viscosity, which resulted in the lowest dominant frequency. Surprisingly, the REL model, which performed well for the time averaged tests, produced rather inconsistent dominant frequency values along the three walls. Conversely, the MW model was quite consistent throughout the cavity. However, it is difficult to judge which performed best at the other locations since no additional experimental data was available. On the other hand, Rossiter's formula applies to the entire cavity and not simply to a specific point. The time history results demonstrate the link between turbulent viscosity and dominant frequency, although it is clear that more parameters affect these results.

FIELD PROPERTIES

The field property results consist of streamlines and the laminar plus turbulent shear stress. These results are quite useful in sorting out the behavior of the respective models and further establish the link between viscosity and quality results.

Figures 8 illustrate the normalized shear stress contours for the various models at a time corresponding to the center aft wall maximum pressure peak. Note that the FL and LIA models are not included as they contain zero Reynolds stresses in the cavity. The first observation is the smoothness of the SBL contours in the shear layer region. In addition, this result contains the greatest shear of all models at the aft cavity corner. Note that the higher stress contours dip into the cavity for this model, unlike any of the other models. Also, note that the REL model effectively reduced the stresses above the cavity, and although identical to the SBL formulation within the cavity, values in that region are considerably lower. Hence, although no change was made to the model within the cavity, the altered flow field behavior drastically changed the shear stress distribution. Therefore, the effect of the REL model is to reduce the overall viscosity in the cavity.

This general trend is also observed in the ISU, SU and FP models. The MW model contained very low values of shear stress inside the cavity, but relatively large, although disjoint as compared to SBL, values outside the cavity. Relative to the REL and SBL models, the MW model provided a much more even distribution of shear stress inside the cavity. These results clearly demonstrate a link between turbulent viscosity and flow properties, but they do not fully explain all appropriate model differences.

The final set of results, shown in figure 9, are the streamlines for each model plotted at the time of maximum center aft wall pressure. Note that in all cases mass ingestion can be observed at the aft cavity wall. The general trends show that increasing viscosity decreases the number of vortices resident in the cavity and the frequency of vortex shedding. Figure 9a shows a distinctly different set of streamlines for the SBL model as compared to the lower viscosity models. In contrast, figure 9f shows a wealth of vortices and indeed inflow separation for the laminar case. Results between these extremes are quite similar as a region of concentrated vorticity appears as a hump roughly halfway across the cavity. A left hand side secondary vortex appears to various degrees in all plots. Corner vortices also appear in several cases.

It is interesting to note that the turbulent viscosity is greatest for the SBL and REL models within the cavity, and that these models produced the smoothest streamlines. In contrast, the FL case produced the greatest number of vortices and rough streamlines.

The results demonstrate a distinct link between eddy viscosity and performance. Overall, the multiple-wall modification appears to provide the best results, although it did not perform best in any one category. It is clear that the turbulent viscosity must be tuned for this application and that the original Baldwin-Lomax model over dissipates the flow. Not shown are results that could be obtained with the myriad combinations of the above models. Baysal et al. [15] reported success with a relaxation/first peak/multiple-wall model, although it is unclear how the combination might perform for all tests. It is also unclear how other standard turbulence models behave for these conditions, in particular, the

Separated Turbulent Flows," AIAA Paper 78-257, January 1978.

[22] Shang, J.S. and Hankey, W.L. Jr., "Numerical Solution for Supersonic Turbulent Flow Over a Compression Ramp," *AIAA Journal*, Vol. 13, pp 1368-1374, October 1975.

[23] Visbal, M. and Knight, D., "The Baldwin-Lomax Turbulent Model for Two-Dimensional Shock-Wave/Boundary-Layer Interactions," *AIAA Journal*, Vol. 22, No. 7, pp 921-928, July 1984.

[24] Degani, D. and Schiff, L.B., "Computation of Turbulent Supersonic Flows around Pointed Bodies Having Crossflow Separation," *Journal of Computational Physics*, Vol. 66, No. 1, pp 173-196, September 1986.

[25] Praharaj, S.C. and Roger, R.P., "Effects of Interference between a Missile and the Front Face of a Separated Booster," AIAA Paper 95-0332, Jan. 1995.

[26] Baysal, O., Private Communication, 1994.

[27] Orkwis, P.D, Tam, C.J. and Disimile, P.J., "Observations on Using Experimental Data as Boundary Conditions for Computations," AIAA Journal, Vol.33, No.1, pp.176-178, Jan. 1995.

MODEL	FORWARD	1/2 FLOOR	2/3 FLOOR	AFT
SBL	13.4	44.6	13.9	13.4
LIA	29.1	40.8	25.9	26.2
FP	27.2	38.8	27.2	27.2
SU	27.2	42.7	27.2	27.2
ISU	27.2	42.7	27.2	27.2
MW	27.2	27.2	27.2	27.2
FL	28.0	41.9	28	28
REL	15.5	42.7	15.5	15.5

TABLE 1 : Dominant Frequencies at Various Cavity Locations (kHz)

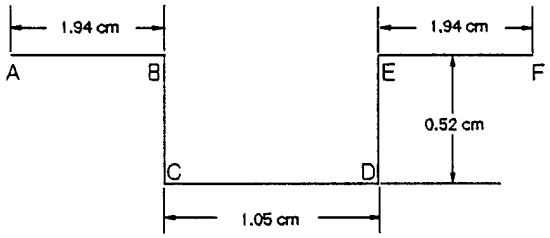

Figure 1 Cavity Geometry.

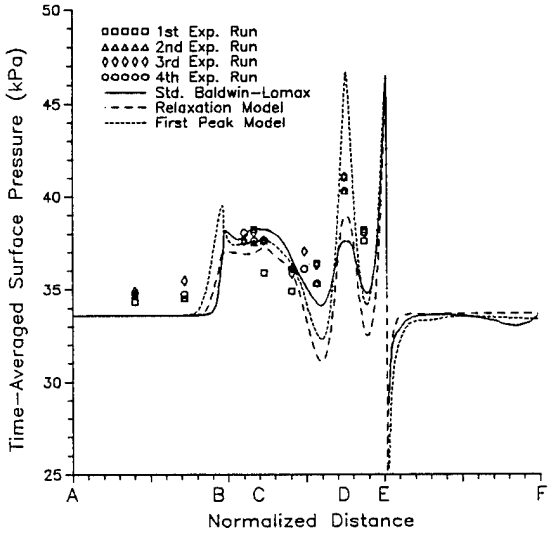

Figure 2a Time Averaged Surface Pressure.

two equation and recently popular RNG based models. However, it is clear that several types of data must be compared to judge the overall effectiveness of a model.

SUMMARY

A study of several modified versions of the Baldwin-Lomax turbulence model applied to 2-D supersonic open cavity flow fields was performed. The results were clearly affected by the levels of turbulent viscosity imposed in the cavity and shear layer regions. The standard Baldwin-Lomax model was found to be the most dissipative and produced the worst overall performance, even when compared to fully laminar computations. The general effect of increased viscosity was a reduction in dominant frequency and overall cavity sound pressure levels. Elimination of turbulent viscosity led to increased resident vortices and unacceptably high dominant frequencies. The tuned damping offered by many of the modifications produced considerable improvements. Although no model performed best in all areas, the multiple-wall modification provided the best overall results.

ACKNOWLEDGEMENTS

The authors wish to thank Dr. Leonidas Sakell and the AFOSR for their generous support through grant #F49620-93-0081. Additional computational resources were provided by the U.S. Army Waterways Experimental Shared Resource Center. Thanks also to Mr. Curt Fox for his editing work.

REFERENCES

[1] Roshko, A., "Some Measurements of Flow in a Rectangular Cutout," NACA Technical Note 3488, August 1955.

[2] McDearmon, R.W., "Investigation of the Flow in a Rectangular Cavity in a Flat Plate at a Mach Number of 3.55," NASA TN D-523, September 1960.

[3] Charwat, A.F., Roos, J.N., Dewey, C.F., and Hitz, J.A., "An Investigation of Separated Flows - Part I: The Pressure Field," *Journal of Aerospace Sciences*, Vol. 28, No. 6, pp 457-470. "Part II: Flow in the Cavity and Heat Transfer," Vol. 28, No. 7, pp 513-527, 1961.

[4] Heller, H. and Bliss, D., "Aerodynamically Induced Pressure Oscillations in Cavities: Physical Mechanisms and Suppression Concepts," AFFDL-TR-74-133, February, 1975.

[5] Hankey, W.L. and Shang, J.S., "Analyses of Pressure Oscillations in an Open Cavity," *AIAA Journal*, Vol. 18, pp 892-898, August 1980.

[6] Borland, C.J., "Numerical Prediction of the Unsteady Flowfield in an Open Cavity," AIAA Paper 77-673, June 1977.

[7] Rossiter, J.E., "Wind Tunnel Experiments on the Flow over Rectangular Cavities at Subsonic and Transonic Speeds," Aeronautical Research Council, R&M No. 3438, 1964.

[8] Cebeci, T. and Smith, A.M.O., *Analysis of Turbulent Boundary Layers*, Academic Press, New York, 1974.

[9] Bradshaw, P., "Effects on Streamline Curvature on Turbulent Flow," AGARDograph No. 169, (AGARD-AG-169), August 1973.

[10] Gorski, J.J., Ota, D.K. and Chakravarthy, S.R., "Calculation of Three Dimensional Cavity Flow Fields," AIAA Paper 87-0117, January 1987.

[11] Suhs, N.E., "Computations of Three-Dimensional Cavity Flow at Subsonic and Supersonic Mach Numbers," AIAA Paper 87-1208, June 1987.

[12] Rizzetta, D.P., "Numerical Simulation of Supersonic Flow Over a Three-Dimensional Cavity," *AIAA Journal*, Vol. 26, No. 7, pp 799-807, July 1988.

[13] Tu, Y., "Unsteady Navier-Stokes Simulations of Supersonic Flow Over a Three-Dimensional Cavity," AIAA Paper 92-2632, June, 1992

[14] Ramakrishnan, S.V., Goldberg, U.C. and Ota, D.K., "Numerical Computation of Hypersonic Turbulent Flows Using Zero- and One-Equation Models," AIAA Paper 89-2234, 1989.

[15] Baysal, O., Yen, G-W and Fouladi, K., "Navier-Stokes Computations of Cavity Aeroacoutics With Suppression Devices," Journal of Vibration and Acoustics, Vol. 116, pp 105-112, January 1994.

[16] Atwood, C.A., "Selected Computations of Transonic cavity Flows," ASME Fluids Engineering Conference, June 1993.

[17] Shih, S-H, "Implicit Procedure for the Solution of the Unsteady Coupled κ-ϵ and Navier-Stokes Equations," Ph. D. Dissertation, University of Cincinnati, 1993.

[18] Disimile, P.J. and Orkwis, P.D., "The Effect of Yaw Angle on the Dominant Frequencies of Rectangular Cavities in Supersonic Flow," to be submitted to AIAA Journal.

[19] Whitfield, D.L., "Implicit Upwind Finite Volume Scheme for the Three-Dimensional Euler Equations," Mississippi State University Report, MSSU-EIRS-ASE-85-1, September 1985.

[20] Simpson, L.B. and Whitfield, D.L., "Flux Difference Split Algorithm for Unsteady Thin-Layer Navier-Stokes Solution," *AIAA Journal*, Vol. 30, No. 4, pp 914-922, April 1992.

[21] Baldwin, B.S. and Lomax, H., "Thin Layer Approximation and Algebraic Model for

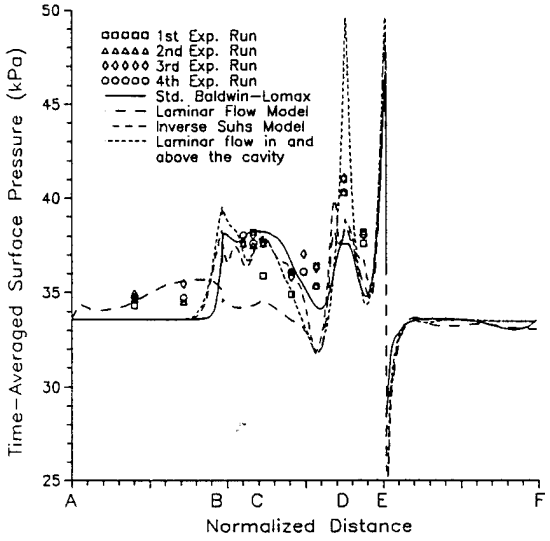

Figure 2b Time Averaged Surface Pressure.

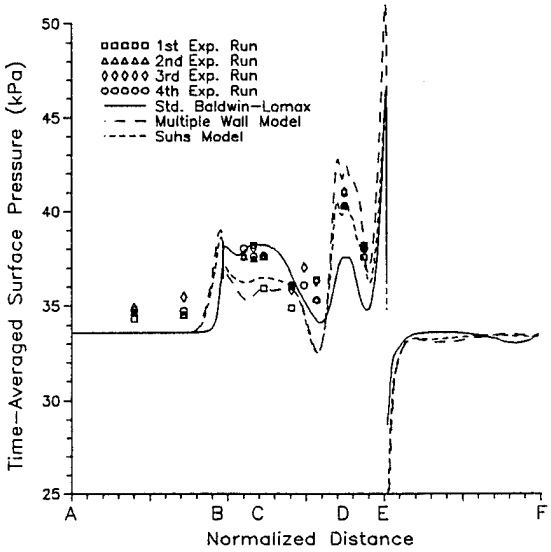

Figure 2c Time Averaged Surface Pressure.

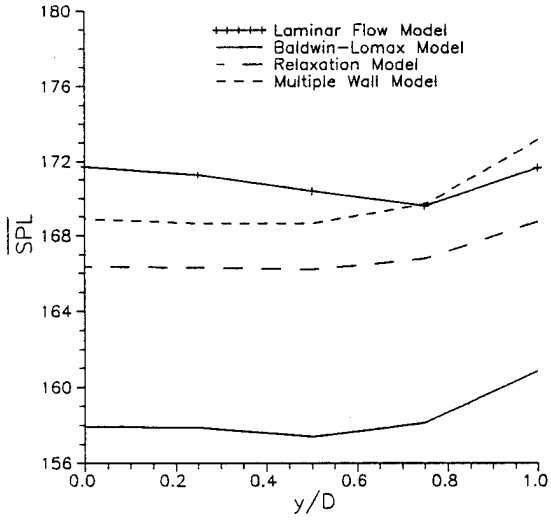

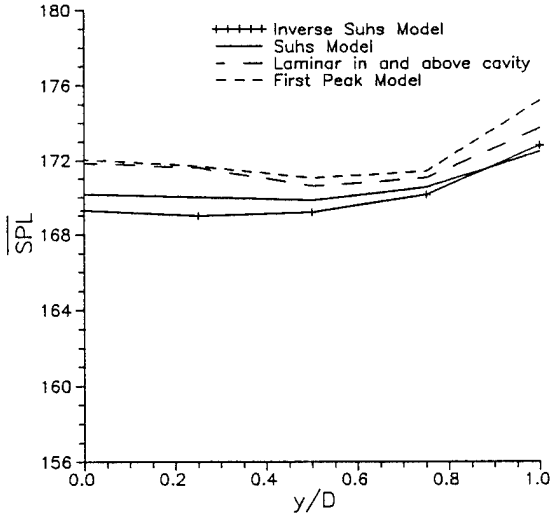

Figures 3a and 3b Time Averaged Sound Pressure Levels Along the Forward Wall.

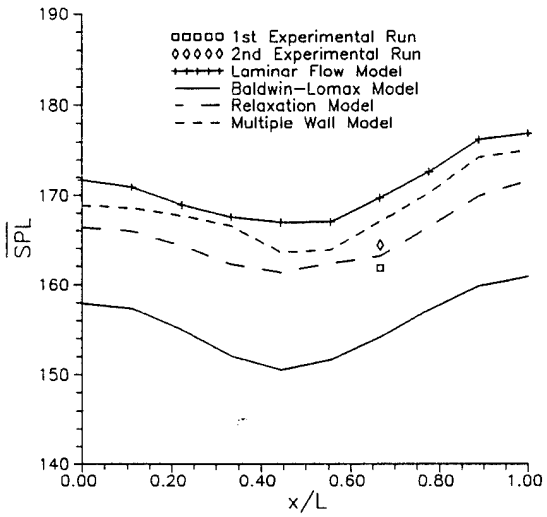

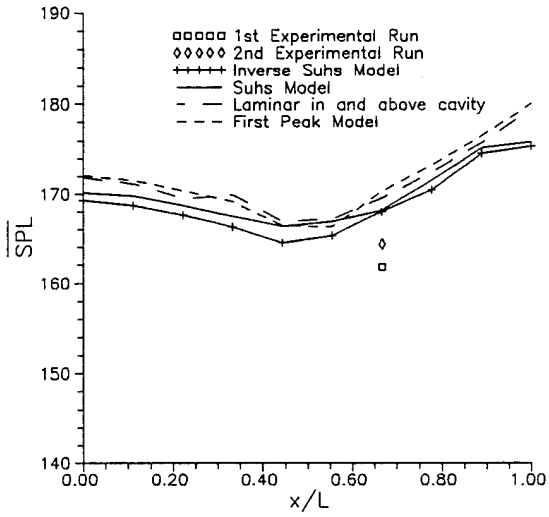

Figures 4a and 4b Time Averaged Sound Pressure Levels Along the Cavity Floor.

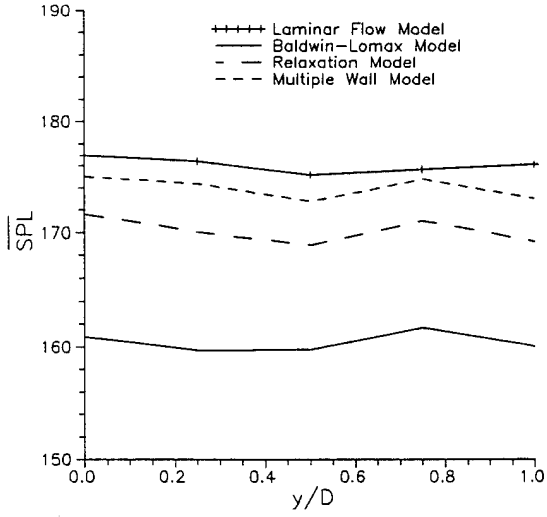

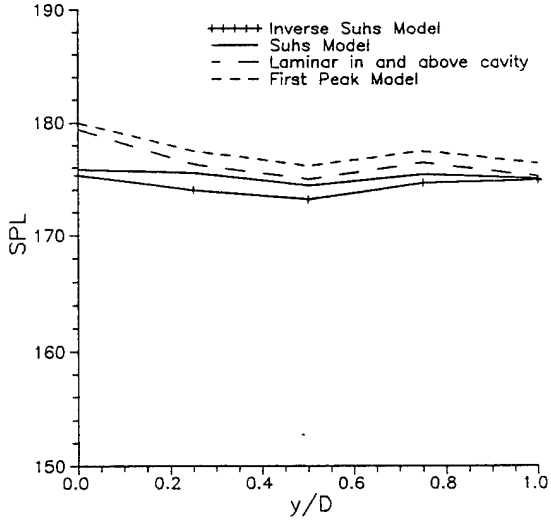

Figures 5a and 5b Time Averaged Sound Pressure Levels Along the Aft Wall.

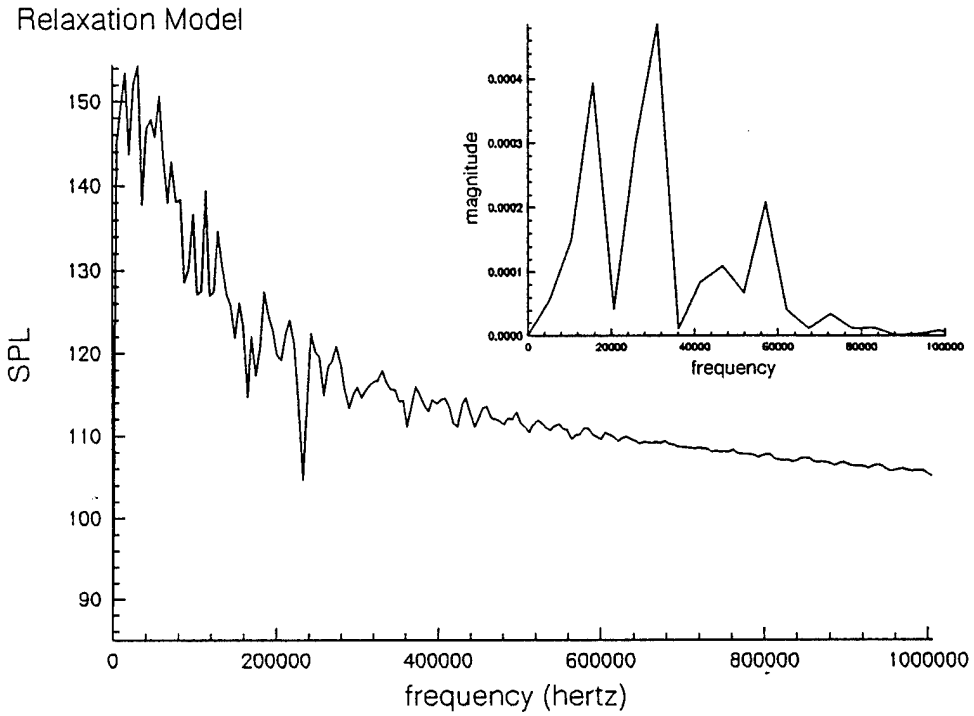

Figure 6 Sound Pressure Levels Versus Frequency and Pressure Perturbation Versus Frequency.

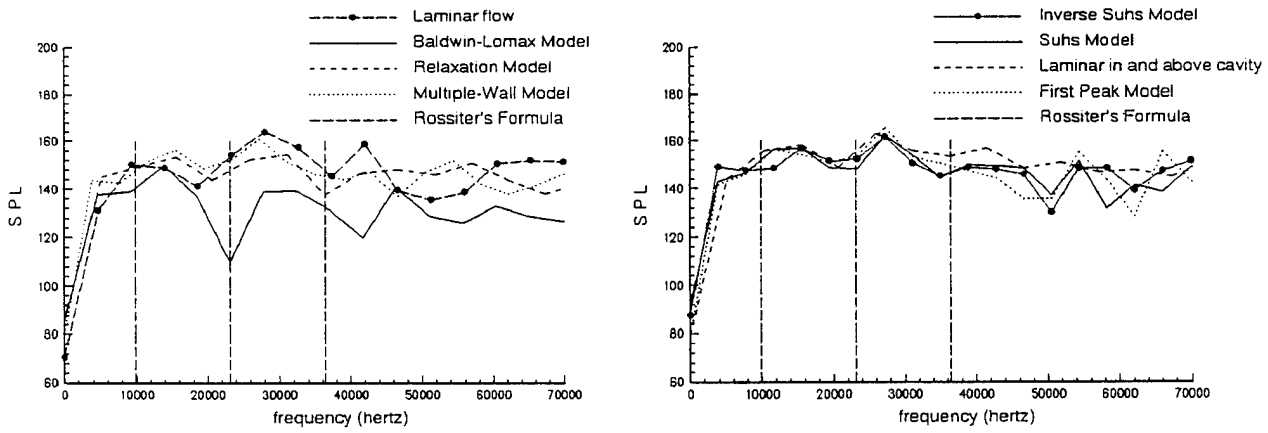

Figures 7a and 7b Sound Pressure Levels FFT's at $\frac{x}{L} = \frac{2}{3}$ Along the Cavity Floor

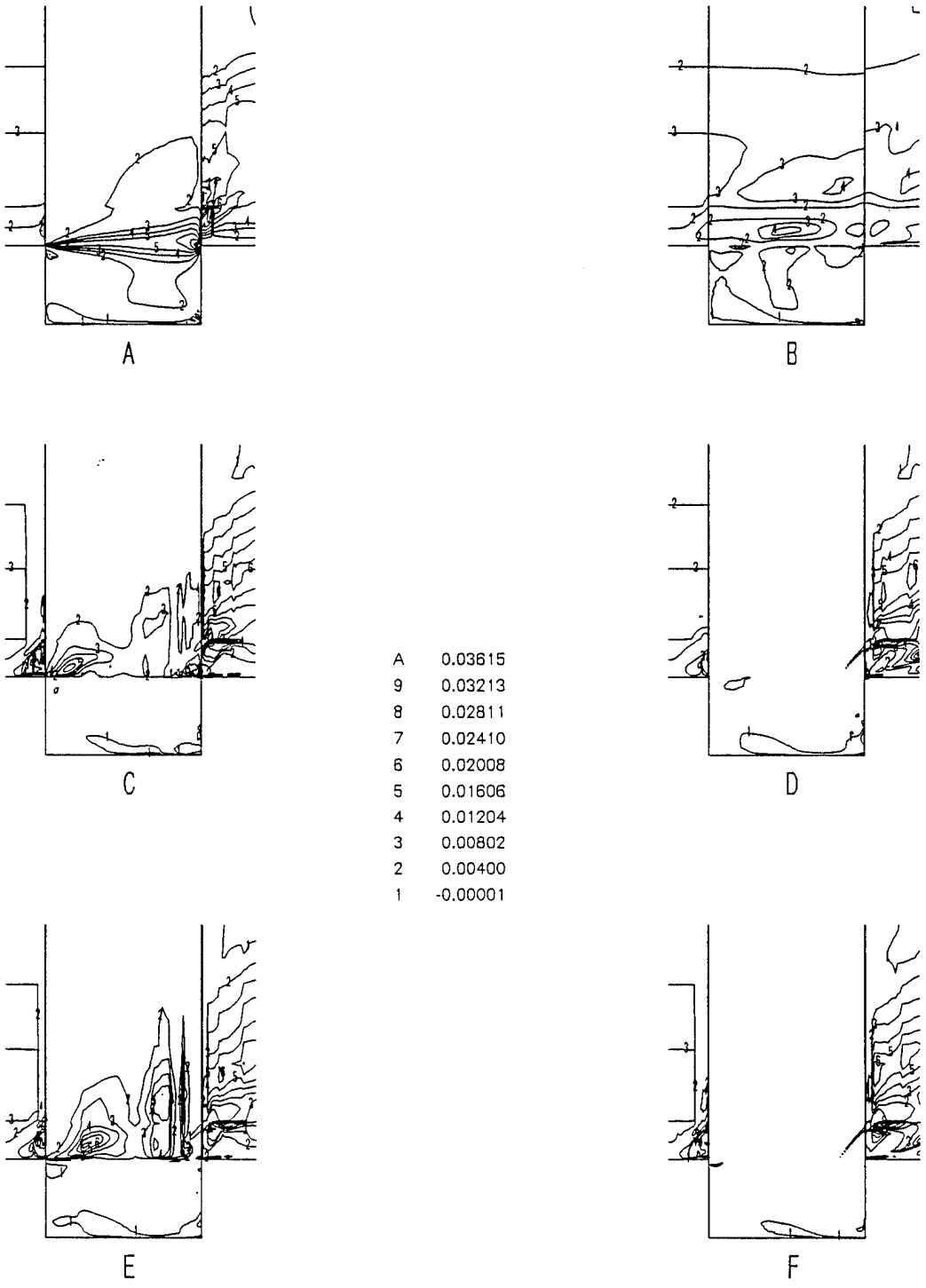

Figure 8 Normalized Shear Stress Contours at Time of Maximum Aft Pressure.

A) SBL, B) REL, C) ISU, D) SU, E) MW, F) FP

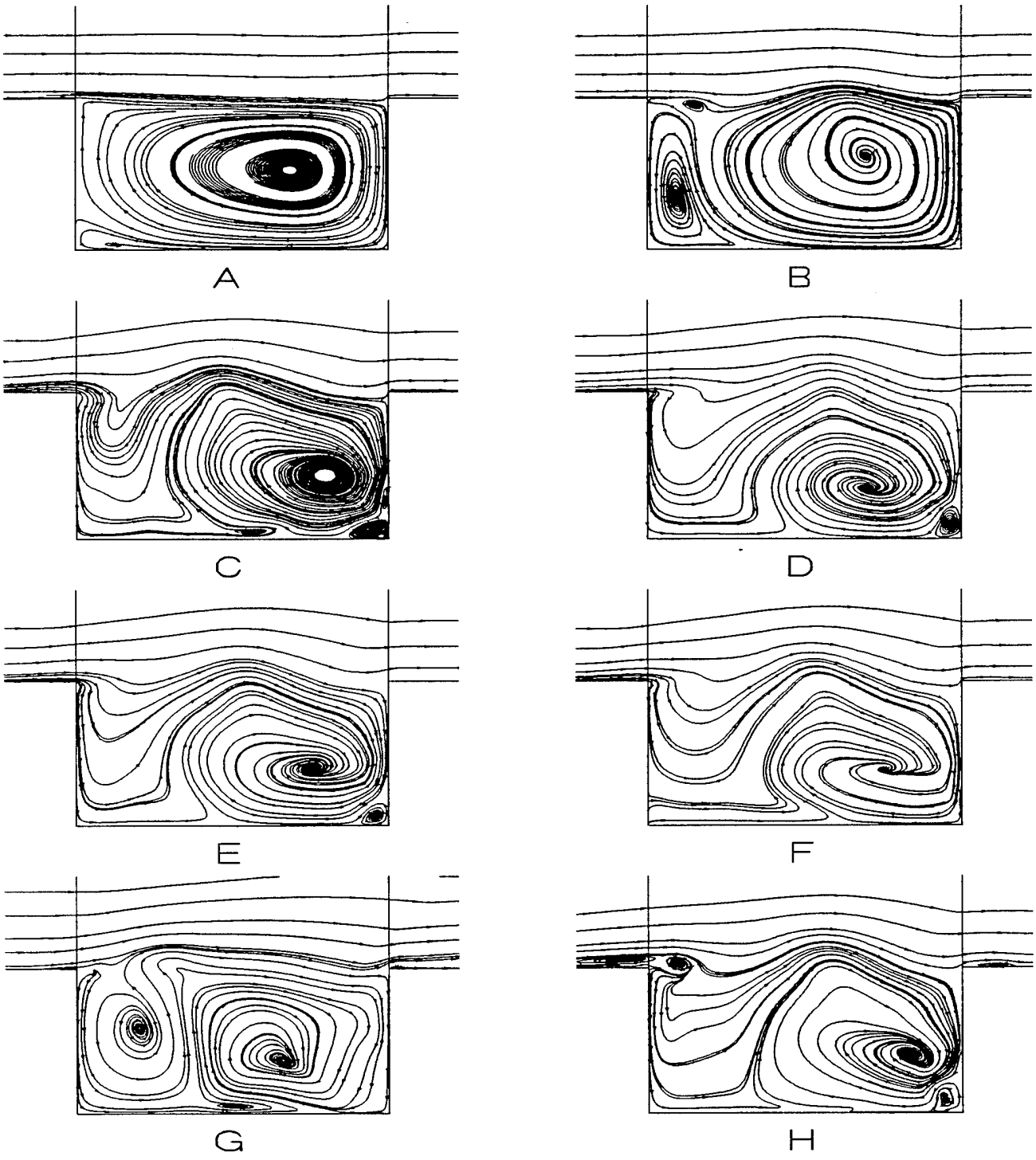

Figure 9. Streamlines at Time of Maximum Aft Pressure.

A) SBL, B) REL, C) ISU, D) SU, E) MW, F) FP, G) LIA, H) FL

A COMPARISON OF BALDWIN-LOMAX TURBULENCE MODELS FOR 2-D OPEN CAVITY COMPUTATIONS

Chung-Jen Tam[1]

Paul D. Orkwis[§]

and

Peter J. Disimile[†]

University of Cincinnati

Cincinnati, Ohio 45221-0070

INTRODUCTION

The presence of a cavity in a surface bounding a fluid flow can cause large pressure, velocity, and density fluctuations in its vicinity as well as propagating acoustic waves. In addition, the drag on the surface can be altered and structural failure due to resonance can occur. A persistent problem with the numerical simulation of cavity flow is the choice of an appropriate turbulence model. Many researchers have opted for the simplicity of the Baldwin-Lomax algebraic model, although many modifications to its basic form have been employed. Suhs[1] applied the standard Baldwin-Lomax model above the up- and downstream flat plates and bottom wall of the cavity, while assuming laminar flow in the region above the cavity. Rizzetta[2] used the Baldwin-Lomax model with the relaxation model[3] for 3-D supersonic open cavity flows. Baysal et al.[4] have researched supersonic open cavity flows using the Baldwin-Lomax turbulence model and a combination of the relaxation modification, the Degani et al.[5] first peak modification, and the multiple-wall modification.

---

[1]Research Assistant, Member AIAA

[§]Assistant Professor of Aerospace Engineering & Engineering Mechanics, Senior Member AIAA

[†]Associate Professor of Aerospace Engineering & Engineering Mechanics, Member AIAA

Although many turbulence model modifications for cavity flow fields have been proposed, little evidence has been offered as to the suitability of a particular choice. Time averaged surface pressure data appear to agree quite well for all models, but apparently different flow field behavior has been reported. This note presents the numerical results[6] of a 2-D open cavity flow field study that employed the double thin-layer Navier-Stokes equations and various versions of the Baldwin-Lomax algebraic turbulence model including the upstream relaxation[2,4], first peak[4], multiple-wall[4], Suhs'[1], and inverse Suhs'[6] approximations as well as two laminar flow approaches. The inverse Suhs' approach consists of the Baldwin-Lomax turbulence model applied above the up- and downstream flat plates and above the cavity, with no turbulence model in the cavity itself. The first laminar flow case utilized the Baldwin-Lomax model only above the up- and downstream flat plates and the second employed laminar flow everywhere in the computational space. The results are compared to the experimental data of Disimile and Orkwis[7].

GOVERNING EQUATIONS

The unsteady Reynolds averaged double thin-layer Navier-Stokes (DTLNS) equations were discretely solved in this work. The DTLNS equations retain the thin layer viscous terms in both the x and y directions as opposed to the thin-layer Navier-Stokes (TLNS) equations which retain terms only in the y direction. The TLNS equations have been described by many researchers[8,9], and as such they will not be included here. The governing equations were solved using a DTLNS modification of the implicit approximate factorization scheme of Simpson and Whitfield[9]. This scheme is second order accurate in both time and space, and employs a Newton-like subiteration procedure. Four subiterations were used in each global iteration with a time step such that the maximum CFL was 0.1.

INITIAL/BOUNDARY CONDITIONS

Boundary conditions were obtained from a flat plate computation that matched the

experimental wind tunnel wall boundary layer momentum thickness (θ) as discussed by Orkwis et al.[10]. The cavity shown in Figure 1 was tested with flow field conditions $M_\infty = 2$, $Re_\theta = 3.69 \times 10^4$ and $\theta = 0.979$ mm. Initially, the flow above the cavity was set equal to the flat plate solution at the location matching the experimental value of θ. The nondimensional initial conditions within the cavity were density and pressure set equal to the wall values, $\rho u = 0.5$, $\rho v = \rho w = 0.0$, and total energy defined from these quantities.

RESULTS AND DISCUSSION

The results are grouped into surface and field properties. The surface properties include time averages of pressure and sound pressure level. Field properties are presented in the form of streamline contours. Comparison of the surface pressure frequency content was performed in an earlier work[6].

The block grid dimensions for this study were 66x55, 66x120 and 66x55 for the upstream, cavity and downstream blocks, respectively, with points clustered along all walls. This choice was based on a grid resolution study, the results of previous researchers, and available computational resources. Half and double x and y direction grid point densities were tested and the fine grid results were only marginally different.

Surface Properties

Figure 2 is a comparison of the time averaged surface pressures obtained from the experiment and the tested turbulence models. The general results can be grouped according to their performance on the forward/bottom walls and the aft wall. The best performers for one case were the worst performers for the other. For example, the best models for the front and bottom walls were the standard Baldwin-Lomax (SBL), inverse Suhs' (ISU), fully laminar (FL), laminar in and above the cavity (LIA), relaxation (REL), and first peak (FP) approaches. The worst performers over this range were the Suhs' (SU) and multiple-wall (MW) models. This situation

was reversed for the aft wall, with SU and MW performing best and SBL, ISU, LIA, REL, FL and FP models performing poorly. This points to the fact that none of these models provide adequate surface pressure results over the entire cavity.

In general, the results do not differ greatly between models. In fact, even the FL computation performed reasonably well on the aft wall. However the FL result contained the most oscillations whereas the SBL result varied in the smoothest fashion. This is a consequence of the turbulent viscosity levels and will be discussed below in greater detail.

Sound Pressure Level

The time histories of the surface pressures were recorded and used to form the time averaged sound pressure level ($\overline{SPL}$) along the cavity floor which is computed by the equation

$$\overline{SPL} = 10 \log_{10}\left(\frac{\overline{p'^2}}{p_{ref}^2}\right) \tag{1}$$

where

$$\overline{p'^2} = \frac{1}{T}\int_{T_1}^{T_2} (p - \bar{p})^2 dt \tag{2}$$

and p_{ref} is the standard reference value, 20 μPa. The comparison with experimental data shown in Figure 3 at $\frac{2}{3}\frac{x}{L}$ along the cavity floor, shows that the REL results agreed best. All of the other approaches were at least 3db from the experimental values, with the SBL giving the maximum difference of 8db.

The surface property results provide clues as to the behavior of the respective turbulence models. It can be conjectured that turbulent viscosity plays an significant role in both the $\bar{p}$ and $\overline{SPL}$ results. Smoother $\bar{p}$ and lower $\overline{SPL}$ values were obtained as the viscous dissipation increased. This general trend is also reflected in the streamline results.

Streamlines

Instantaneous streamline results are quite useful in sorting out the behavior of the respective

models and further establishing the effect of viscosity. Figure 4 illustrates the streamlines for each model plotted at the time of maximum center aft wall pressure. Note that in all cases mass ingestion can be observed at the aft cavity wall. The general trends show that increasing viscosity decreases the number of vortices resident in the cavity and the frequency of vortex shedding[6]. Figure 4a shows a distinctly different flow field topology for the SBL model as compared to the lower viscosity models. In contrast, figure 4f shows a wealth of vortices and indeed inflow separation for the FL case. Results between these extremes are quite similar. A left hand side secondary vortex appears to various degrees in all plots. Corner vortices appear in several cases.

SUMMARY

A study of several modified versions of the Baldwin-Lomax turbulence model applied to 2-D supersonic open cavity flow fields was performed. The results were clearly affected by the levels of turbulent viscosity imposed in the cavity. The standard Baldwin-Lomax model was found to be the most dissipative and produced the worst overall performance, even when compared to fully laminar computations. The general effect of increased viscosity was a reduction in dominant frequency and overall cavity sound pressure levels. Elimination of turbulent viscosity led to increased resident vortices and unacceptably high dominant frequencies. The tuned damping offered by many of the modifications produced considerable improvements. Although no model performed best in all areas, the multiple-wall modification provided the best compromise. Combinations of the models might produce a better result.

ACKNOWLEDGEMENTS

The authors wish to thank Dr. Leonidas Sakell and the AFOSR for their generous support through grant #F49620-93-0081. Computational resources were provided by the U.S. Army Waterways Experimental Shared Resource Center.

REFERENCES

[1]Suhs, N.E., "Computations of Three-Dimensional Cavity Flow at Subsonic and Supersonic Mach Numbers," AIAA Paper 87-1208, June 1987.

[2]Rizzetta, D.P., "Numerical Simulation of Supersonic Flow Over a Three-Dimensional Cavity," *AIAA Journal*, Vol. 26, No. 7, 1988, pp. 799-807.

[3]Bradshaw, P., "Effects of Streamline Curvature on Turbulent Flow," AGARDograph No. 169, (AGARD-AG-169), August 1973.

[4]Baysal, O., Yen, G-W., and Fouladi, K., "Navier-Stokes Computations of Cavity Aeroacoutics With Suppression Devices," *Journal of Vibration and Acoustics*, Vol. 116, Jan. 1994, pp. 105-112.

[5]Degani, D. and Schiff, L.B., "Computation of Turbulent Supersonic Flows around Pointed Bodies Having Crossflow Separation," *Journal of Computational Physics*, Vol. 66, Sept. 1986, pp. 173-196.

[6]Tam, C.-J., Orkwis, P.D., and Disimile, P.J., "A Comparison of Several Standard Turbulence Models for 2-D Open Cavity Flow Field Computations," AIAA Paper 95-0361, Jan. 1995.

[7]Disimile, P.J. and Orkwis, P.D., "The Effect of Yaw Angle on the Dominant Frequencies of Rectangular Cavities in Supersonic Flow," to be submitted to AIAA Journal.

[8]Whitfield, D.L., "Implicit Upwind Finite Volume Scheme for the Three-Dimensional Euler Equations," Mississippi State University Report, MSSU-EIRS-ASE-85-1, Sept. 1985.

[9]Simpson, L.B. and Whitfield, D.L., "Flux Difference Split Algorithm for Unsteady Thin-Layer Navier-Stokes Solution," *AIAA Journal*, Vol. 30, April 1992, pp. 914-922.

[10]Orkwis, P.D, Tam, C.J. and Disimile, P.J., "Observations on Using Experimental Data as Boundary Conditions for Computations," *AIAA Journal*, Vol.33, Jan. 1995, pp.176-178.

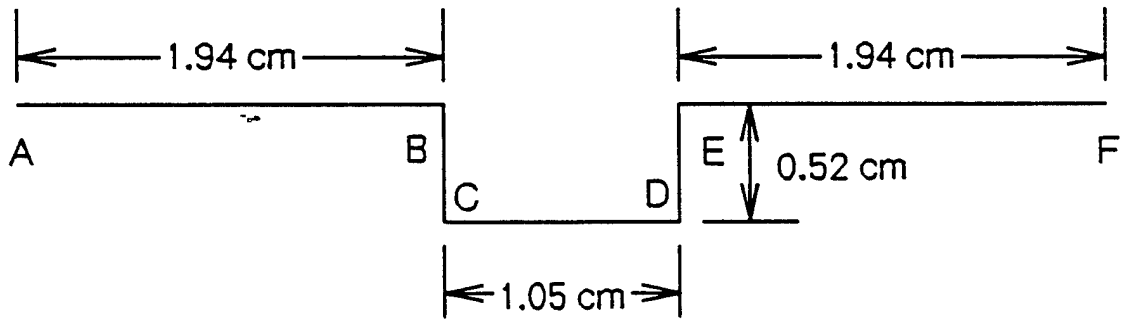

Figure 1. Cavity Geometry

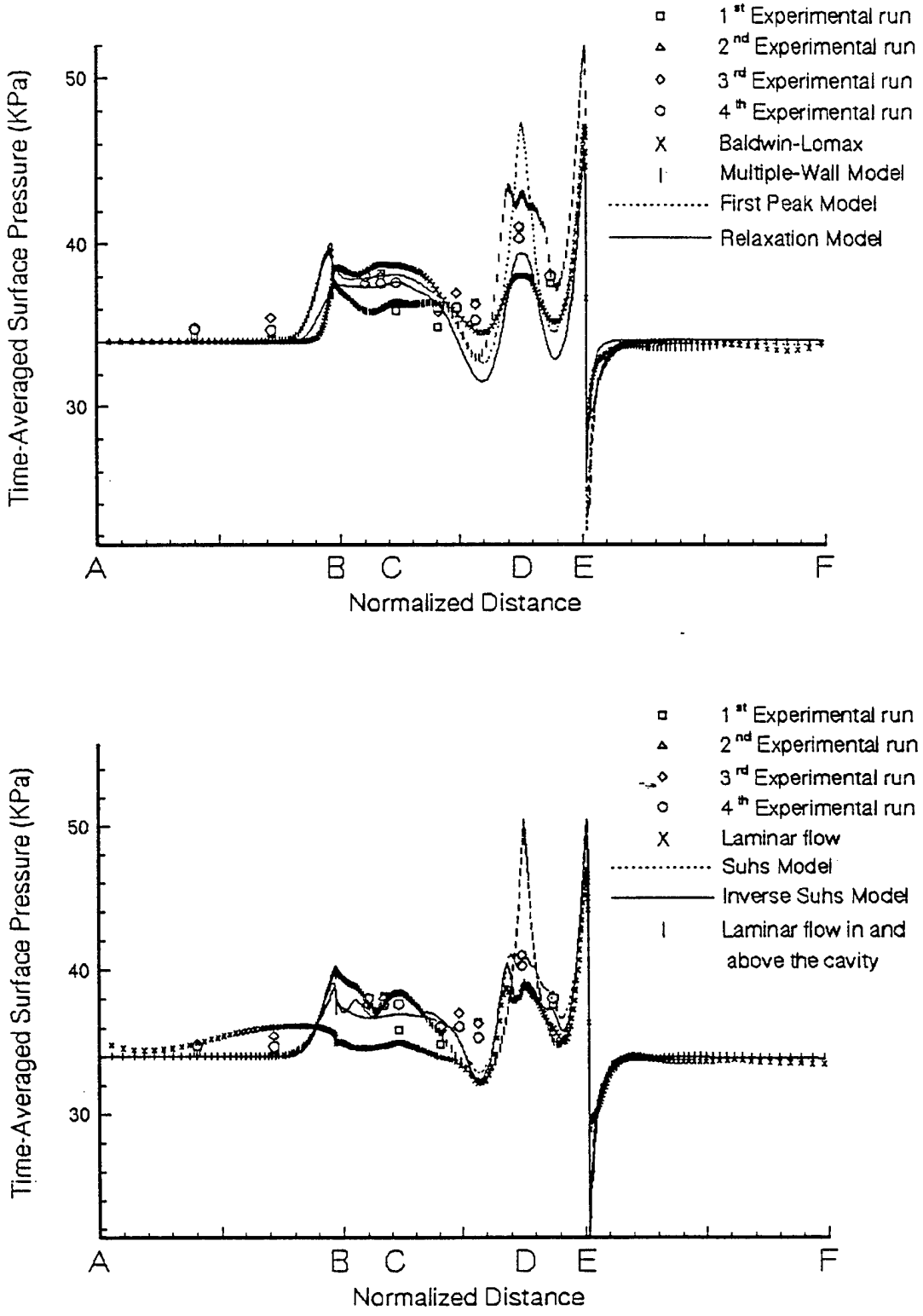

Figure 2. Time-Averaged Surface Pressure

SUPERSONIC OPEN CAVITY FLOW PHYSICS ASCERTAINED FROM ALGEBRAIC TURBULENCE MODEL SIMULATIONS

by
Paul D. Orkwis*
Peter J. Disimile†
and
Chung-Jen Tam‡
University of Cincinnati
Cincinnati, Ohio

Abstract

The proposed paper will describe the flow physics inherent in supersonic open cavities as simulated by temporally second order accurate double thin layer Navier-Stokes equation computations that employ a modified version of the Baldwin-Lomax turbulence model. A cavity oscillation cycle will be presented that unites those proposed previously by Heller and Bliss, and Rockwell et al. In the current work, the turbulence model includes the upstream relaxation, multiple wall and nearest peak modifications; an approach similar to that employed by Baysal. This model was shown previously by the authors to provide the best overall experimental data match amongst those reported by past authors. Time histories of streamlines, and contours of pressure and vorticity will be presented to illustrate the cycle. Simplified sketches will be included to help visualize important aspects of the flow.

Introduction

The fundamental details of supersonic open cavity flow fields are of interest because cavities exist on virtually all high speed attack, fighter and recon-

*Senior Member AIAA, Assistant Professor of Aerospace Engineering & Engineering Mechanics
†Member AIAA, Associate Professor of Aerospace Engineering & Engineering Mechanics
‡Member AIAA, Research Assistant

naissance aircraft. Increased drag, high heat transfer rates and structurally damaging oscillations are associated with these flow fields. In addition, stores are expected to be launched from such an environment making a through understanding of the flow field details important.

The basic physical structure of cavity flow fields can be described as either closed, open or transitioning [1,2,3,4]). Closed cavities are typically long and shallow with a length to depth ratio (L/D) greater than 13. They are characterized by a shear layer that impinges on the cavity floor producing two large recirculation regions. Closed cavities are associated with high drag coefficients [5,6,7,8] and heat transfer properties [9,10,11,12] as compared to open cavities, as such, they are less desirable. Open cavities are short and deep with an L/D less than 10. They contain shear layers that span the cavity and are more typical of those found in aircraft applications. Open cavity flow fields are remarkably complicated with internal and external regions that are coupled via self sustained shear layer oscillations. Coherent shed vorticity, unsteady weak shock or pressure waves, and interactions between the shed vortices and the vortices that reside in the cavity are also present. Flow field characteristics appear to depend primarily upon the shape of the cavity and the Mach number, with Reynolds number effects considered to be less important.

Several issues remain to be understood for open cavity flow fields. Researchers appear to agree that an oscillating shear layer exists, that the primary and secondary vortices residing within the cavity are driven by the shear layer, that a mass "breathing" effect occurs within the cavity, and that pressure oscillations exist. However, the mechanisms driving this flow field have not yet been agreed upon.

Notable experimental efforts by Rossiter [13], Rockwell et al. [14, 15], and Heller and Bliss [16] have attempted to determine some of these details. Rossiter employed dimensional analysis and empiricism to produce the following formula for the cavity resonance frequencies

$$f = \frac{U}{L}\frac{(m-\gamma)}{\left(\frac{1}{K}+M\right)}$$

Where U is the freestream velocity, L the cavity length, M the Mach number, m an integer (1,2,3, ...), and γ and K are constants. Rossiter's formula predicts the dominant frequency of the cavity oscillation with remarkable accuracy, as demonstrated previously by the authors [18]. This number can also be obtained from numerical simulations and is one of the more appropriate accuracy metrics for this unsteady flow. Rossiter's model was derived using an edge tone analogy and the assumption that the acoustic radiation is due to shed vortices impinging on the aft cavity wall. His experiments visualized the shed vortices and the pressure waves external to the cavity, although they did not visualize the standing waves described as existing within the cavity. This work laid the foundation for the more comprehensive theories regarding cavity resonance put forth by Heller and Bliss [16], and Rockwell et al. [14,15].

Rockwell et al. and others [14,15,19] provide an explanation of the cavity resonance cycle which stipulates that the shear layer oscillation is driven primarily by transient vortex motions within the cavity. They contend that the vortices which form within the oscillating shear layer sometimes impinge upon the aft wall and then mix with vortices inside the cavity. The shear layer vortex/edge interaction adds mass to the cavity; the "breathing-in" phase. This captured vortex then interacts with the internal cavity vortices, displacing them and producing pressure oscillations within the cavity. These fluctuations travel forward and eventually displace the shear layer at the leading edge. This produces an external excitation of the shear layer that initiates the shedding of another vortex and closes the feedback loop.

A second mechanism, proposed by Heller and Bliss [16] and cited by several other researchers [20,23], defines the shear layer oscillation cycle as dependent upon unsteady planar compression waves. Once again the cycle begins with the unstable shear layer detaching from the trailing edge and impinging on the aft wall of the cavity. Mass enters the cavity in a fashion similar to the previous explanation. A normal shock wave forms and is convected upstream. This shock wave is accompanied by an inviscid region shock wave which equalizes the pressure across the shear layer. The internal shock eventually hits the forward wall and is reflected back into the cavity. The pressure doubling behind the reflected shock displaces the shear layer and initiates a new shed vortex. The reflected shock passes through new forward moving shocks as it travels towards the aft wall. The inviscid region shock wave no longer exists since the external flow is subsonic relative to the internal shock wave motion. The cycle is completed when the reflected shock hits the aft wall; expelling mass from the cavity in the "breathing out" phase.

It should be noted that although the two descriptions appear to be quite different, the two points of view are not mutually exclusive. In fact, there appears to be some truth to both explanations, although, as discussed later, some common misconceptions as well.

Later researchers have produced considerable computational evidence regarding the nature of the cavity resonance cycle. Hankey and Shang [20], Rizzetta [23], Tu [21], Suhs [22], Baysal and Stallings [24], Morgenstern and Chokani [25], Orkwis et al. [17], and Tam et al. [18] have all attempted to simulate the open cavity resonance cycle. All of these efforts employed a Reynolds averaged Navier-Stokes (RANS) equation approach with an algebraic turbulence model. More advanced turbulence models, such as one [26] and two equation [27] models, have also been attempted, although with no greater success. The general results indicate that a wide variety of solutions can be obtained with the various turbulence models, but that the large scale features are similar for the best performing models. Good results are typically obtained for time averaged surface properties like pressure and shear stress, but unsteady properties like sound pressure levels (SPLs) and cavity resonance frequency are not computed consistently. This is perhaps not surprising since turbulence models are not typically tuned to unsteady applications.

An extensive test of the algebraic turbulence modeling modifications was conducted previously by the authors [18]. The modifications judged most effective by virtue of accurate SPL comparisons were combined and employed in the current work. These models, in general, reduced considerably the overall turbulent viscosity levels in the cavity. This is, of course, a problem with virtually all RANS based simulations of unsteady flows, since turbulence modeling has not been directed in a meaningful way toward these problems. Because of this direct numerical simulation of the turbulence or large eddy simulation would be more appropriate approaches for this class of flows. However, the results obtained with the algebraic turbulence models appear to model the large scale features of the flow reasonably well and can be used to provide some insight into the mechanisms that lead to the cavity resonance cycle.

With the above caveat in mind, the flow physics of supersonic open cavities will be examined in the proposed paper. The following sections provide a rough draft of the expected paper and describe the employed discrete governing equations, the numerical algorithm, the accuracy of the results, preliminary results for the computed cavity flow field, and a description of the expected results to be included in the final draft of the paper.

Governing Equations

The equations solved discretely in this work are the double thin layer Navier-Stokes (DTLNS) equations. These differ from the typical thin layer equations by retaining terms in both the normal and axial directions. This modification makes sense for cavities since they contain both horizontal and vertical walls. The equations will be included in the final paper.

Numerical Method

The governing equations were discretely solved via a DTLNS version of the multi-block finite volume scheme developed by Simpson and Whitfield [28]. The current procedure was detailed in earlier works by the authors [17,18] and will not be included in the paper. The scheme utilizes Roe flux difference splitting for the residual and an approximate Steger-Warming splitting for the Jacobian matrix. **The scheme is third order accurate in space and second order accurate in time** when a Newton-like subiteration procedure is employed [28]. Four subiterations per global iteration were used as this reduces the subiteration residual sufficiently to attain second order temporal accuracy.

The turbulence model for this run was a version of the Baldwin-Lomax model modified to employ upstream relaxation and multiple walls, and to choose the nearest peak of the F function. Details of the scheme were described previously by the authors [18] and will not be discussed further in this draft. An appropriately detailed description will be included in the final paper.

Grids for the computation utilized typical boundary layer clustering about all walls and throughout the shear layer region. Three blocks were employed such that the cavity and shear layer were contained in the same block. Block 1 included the region above the upstream flat plate, block 2 the cavity region and block 3 the region above the downstream flat plate. The block grids had dimensions of 66x55, 66x120 and 66x55 respectively. A grid resolution study was performed in the previous research to arrive at these choices. The grid and the clustering function will be included in the final paper.

Boundary and Initial Conditions

Boundary conditions for the computation were prescribed on the inflow plane, no-slip on solid surfaces, and outflow conditions on exit boundaries. The upstream profile was determined from a flat plate computation from which the proper profile was chosen by finding the x-location profile with the same momentum thickness as that found experimentally for the cavity [18]. A computational approach is required because experimental measurements do not provide sufficient information (i.e. no v-velocity) to fully prescribe the inflow, as detailed previously by the authors [17].

Initial conditions for the flow field were obtained by prescribing the inflow profile for points outside of the cavity. Flow inside the cavity was set by using the wall pressure and density, x-momentum one half the freestream, and y and z momentum equal zero.

Results

The emphasis of the proposed paper will lie in the presentation and discuss of the computed solution. This section describes the test conditions, presents several aspects of the results and discusses how they will be utilized and probed to determine the cavity flow physics. This analysis has not yet been performed in detail, as such, only the preliminary findings will be included in this initial draft. However, all computed results to be included in the paper are provided.

Results were obtained to match the experimental data taken previously [17] for flow about an L/D = 2 quasi-two-dimensional cavity. The test parameters were $M_\infty = 2$, $Re_\theta = 3.69 \cdot 10^4$ and $\theta = 0.979mm$. The computation was run 36 characteristic times after the initial transients were purged. No additional computations are planned for the final version of the paper.

Preliminary Results

Results include time histories of all solution variables. Two cavity oscillation cycles have been plotted in the form of the streamlines, pressure contours and vorticity contours found in figures 1, 2 and 3. The initial impression of the streamlines appears to indicate that a vortex is shed from

the forward wall of the cavity, convects downstream and joins with the cavity resident vortex. It later tears away from this vortex and is convected out of the cavity. Another vortex is in the process of shedding as the original vortex prepares to exit the cavity. No other significant vortex interactions are apparent in the streamline plots, although several corner vortices appear at different times. The plots also indicate that the second cycle is virtually the same as the first, even though identical frames were not captured.

The pressure contours indicate the presence of several external shock waves apparently tied to undulations in the shear layer. These waves enter the cavity, but appear to spread significantly and no longer mimic discontinuities. A standing compression wave appears to develop before the aft wall, although it is not apparent that it convects upstream in the manner described by Heller and Bliss. In addition, the initiation of the corner vortex does not appear to be tied to the impingement of a forward moving wave. In fact, the opposite appears to be true, although the pressure does rise when the shed vortex is disconnected from the shear layer. Several external flow "cells" appear that contain both high and low pressure regions. These cells seem to be tied to the shear layer undulations and not to internal compression waves.

Preliminary vorticity results clearly illustrate the shedding of the corner vortex. In addition, the impingement of this vortex on the rear wall and its consequent tearing are vividly portrayed. The impinging vortex is shred into a part that convects downstream and another which is ingested by the cavity. The ingested portion appears to be convected downward and forward by the resident vortex until it reaches the approximate center of the cavity. At that point it begins to travel upward causing (because of ?) the presence of a vortex near the center of the cavity floor. The vortex appears to move behind the new shed vortex and follow it out the cavity. It does not appear to be the reason for the shredding of the new shed vortex from the shear layer vorticity sheet, but it does appear to be closely tied to this event. In any case, it is not related to the formation of the shed vortex.

Expected Results

The full paper will include a more detailed analysis of these results with a special emphasis on the features that are responsible for the cavity resonance cycle. In particular, the pressure waves will be mapped and sketches made to detail the features present during the oscillation cycle. These pressure wave sketches will be compared to those presented by Heller and Bliss and then used to help explain the resonance cycle. The vorticity contours will be used to sketch the locations and relative strengths of the shed and resident vortices. The dynamics of the individual vortices will be sketched and discussed separately. These results will then be contrasted with the resonance cycle described by Rockwell et al. Close correlation between the two sets of sketches will be the basis of a new description of the resonance

cycle. Particular attention will be paid to understanding which phenomena precede which, and to how they affect one another. The origins of the cavity oscillation will then emerge.

Summary

The proposed paper will describe an analysis of the flow physics inherent in supersonic open cavities as computed through simulations of the double thin layer Navier-Stokes equations. Time histories of streamlines, pressure contours and vorticity contours will be used to define the cavity resonance cycle. This explanation will be compared and contrasted to the widely discussed resonance cycles described by Heller and Bliss, and Rockwell et al. Sketches of pressure wave motions and vortex locations and strengths will be included. Insight will be gained as to the fundamental fluid dynamic mechanisms responsible for cavity oscillations.

References

[1] Roshko, A. "Some Measurements of Flow in a Rectangular Cutout," NACA Technical Note 3488, 1955.

[2] McDearmon, R.W., "Investigation of the Flow in a Rectangular Cavity in a Flat Plate at a Mach Number of 3.55," NASA TN D-523, Sept. 1960.

[3] Tracy, M.B., Plentovich, E.B., and Chu, J., "Measurements of Fluctuating Pressure in a Rectangular Cavity in Transonic Flow at High Reynolds Numbers," NASA TM 4363, June 1992.

[4] Tracy, M.B. and Plentovich, E.B., "Characterization of Cavity Flow Fields Using Pressure Data Obtained in the Langley 0.3-Meter Transonic Cryogenic Tunnel," NASA TM 4436, March 1993.

[5] Charwat, A.F., Roos, J.N., Dewey, C.F. and Hitz, J.A., "An Investigation of Separated Flows - Part I: The Pressure Field," *Journal of Aerospace Sciences*, Vol. 28, No. 6, pp 457-470. "Part II: Flow Separation in the Cavity and Heat Transfer," Vol. 28, No. 7, pp 513-527, 1961.

[6] McGregor, O.W. and White, R.A., "Drag of Rectangular Cavities in Supersonic and Transonic Flow Including the Effect of Cavity Resonance," *AIAA Journal*, Vol. 8, No. 11, pp 1959-1964, Nov. 1970.

[7] Catani, U., Bertin, J.J., DeAmicis, R., Masullo, S. and Bouslog, S.A., "Aerodynamic Characteristics for a Slender Missile with Wrap-Around Fins," *Journal of Spacecraft and Rockets*, Vol. 20, No. 2 March-April 1983.

[8] Blair, A.B., Jr. and Stallings, R.L., Jr., "Supersonic Axial Force Characteristics of a Rectangular Box Cavity with Various Length-to-Depth Ratios in a Flat Plate," NASA TM-87659, 1986.

[9] Hahn, M., "Experimental Investigation of Separated Flow over a Cavity at Hypersonic Speed," *AIAA Journal*, Vol. 7, No. 6, June 1969.

[10] Nestler, D.E., Saydah, A.R. and Auxler, W.L., "Heat Transfer to Steps and Cavities in Hypersonic Turbulent Flow," *AIAA Journal*, Vol. 7, No. 7, July 1969.

[11] White, R.A., "Some Results on the Heat Transfer within Resonant Cavities at Subsonic and Supersonic Mach Numbers," *ASME Journal of Basic Engineering*, Vol. 12, pp 537-542.

[12] Nestler, D.E., "An Experimental Study of Hypersonic Cavity Flow," *Journal of Spacecraft and Rockets*, Vol. 19, No. 3, May-June 1982.

[13] Rossiter, J.E., "Wind Tunnel Experiments on the Flow over Rectangular Cavities at Subsonic and Transonic Speeds," ARC R&M No. 3438, 1966.

[14] Rockwell, D. and Knisely, C., "The Organized Nature of Flow Impingement Upon a Corner," *Journal of Fluid Mechanics*, Vol. 93, Part 3, 1970, pp 413-432.

[15] Rockwell, D. and Naudascher, E., "Review- Self Sustaining Oscillations of Flow Past Cavities," *Journal of Fluids Engineering*, Vol. 100, June 1978, pp 152-165.

[16] Heller, H. and Bliss, D., " Aerodynamically Induced Pressure Oscillations in Cavities: Physical Mechanisms and Suppression Concepts," AFFDL-TR-74-133, February 1975.

[17] Orkwis, P.D., Tam, C.-J., and Disimile, P.J., "Observations on Using Experimental Data as Boundary Conditions for Computations," *AIAA Journal*, Vol. 33, No. 1, January 1995, pp. 176-178.

[18] Tam, C.-J., Orkwis, P.D., and Disimile, P.J., "A Comparison of Several Standard Turbulence Models for 2-D Open Cavity Flow Field Computations," AIAA Paper 95-0361, AIAA 33rd Aerospace Sciences Meeting, Reno, NV, January 1995.

[19] Zhang, X. and Edwards, J.A., "Computational Analysis of Unsteady Supersonic Cavity Flows Driven by Thick Shear Layers," *Aeronautical Journal*, pp 365-374, Nov. 1988.

[20] Hankey, W.L. and Shang, J.S., "Analyses of Pressure Oscillations in an Open Cavity," *AIAA Journal*, Vol. 18, No. 8, August 1980, pp. 892-898.

[21] Tu, Y., "Unsteady Navier-Stokes Simulations of Supersonic Flow Over a Three-Dimensional Cavity," AIAA Paper 92-2632, June 1992.

[22] Suhs, N.E., "Unsteady Computations for a Three-Dimensional Cavity With and Without an Acoustic Suppression Device," AIAA Paper 93-3402-CP, (1993).

[23] Rizzetta, D.P., "Numerical Simulation of Supersonic Flow Over A Three-Dimensional Cavity," *AIAA Journal*, Vol. 26, No. 7, July 1988, pp 799-807.

[24] Baysal, O. and Stallings, R.L., "Computational and Experimental Investigation of Cavity Flowfields," *AIAA Journal*, Vol 26, No.1, January 1988, pgs 6 & 7.

[25] Morgenstern, A. Jr., and Chokani, N., "Hypersonic Flow Past Open Cavities," *AIAA Journal*, Vol. 32, No. 12, December 1994, pp 2387-2393.

[26] Ramakrishnan, S.V., Goldberg, U.C., and Ota, D.K., "Numerical Computation of Hypersonic Flows Using Zero- and One-Equation Models," AIAA Paper 89-2234, 1989.

[27] Gorski, J.J., Ota, D.K., and Chakravarthy, S.R., "Calculation of Three Dimensional Cavity Flow Fields," AIAA Paper 87-1208, June 1987.

[28] Simpson, L.B., and Whitfield, D.L., "Flux Difference Split Algorithm for Unsteady Thin-Layer Navier-Stokes Solutions," *AIAA Journal*, Vol. 30, No. 4, April 1992, pp 914-922.

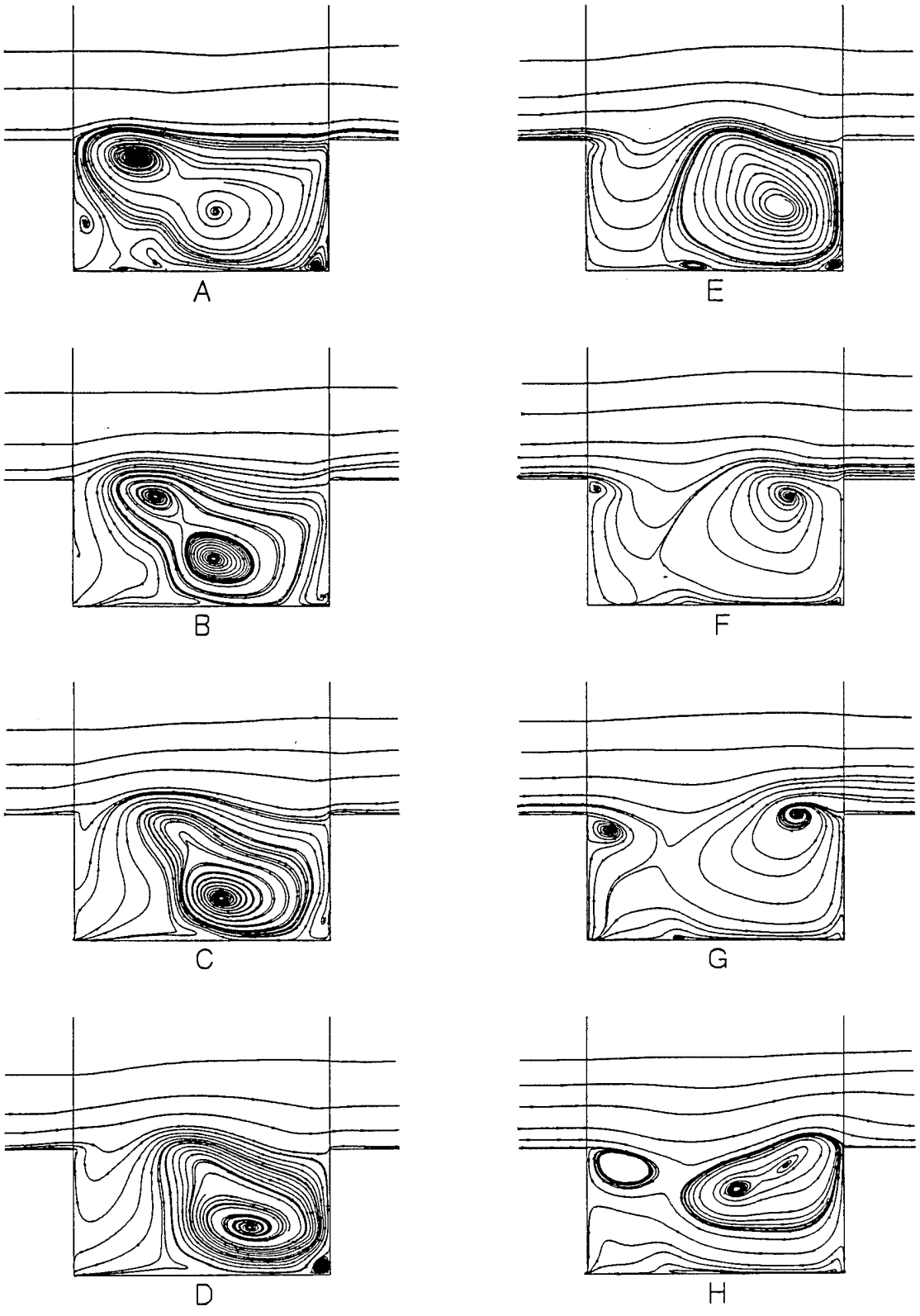

Time series streamline

Figure 1

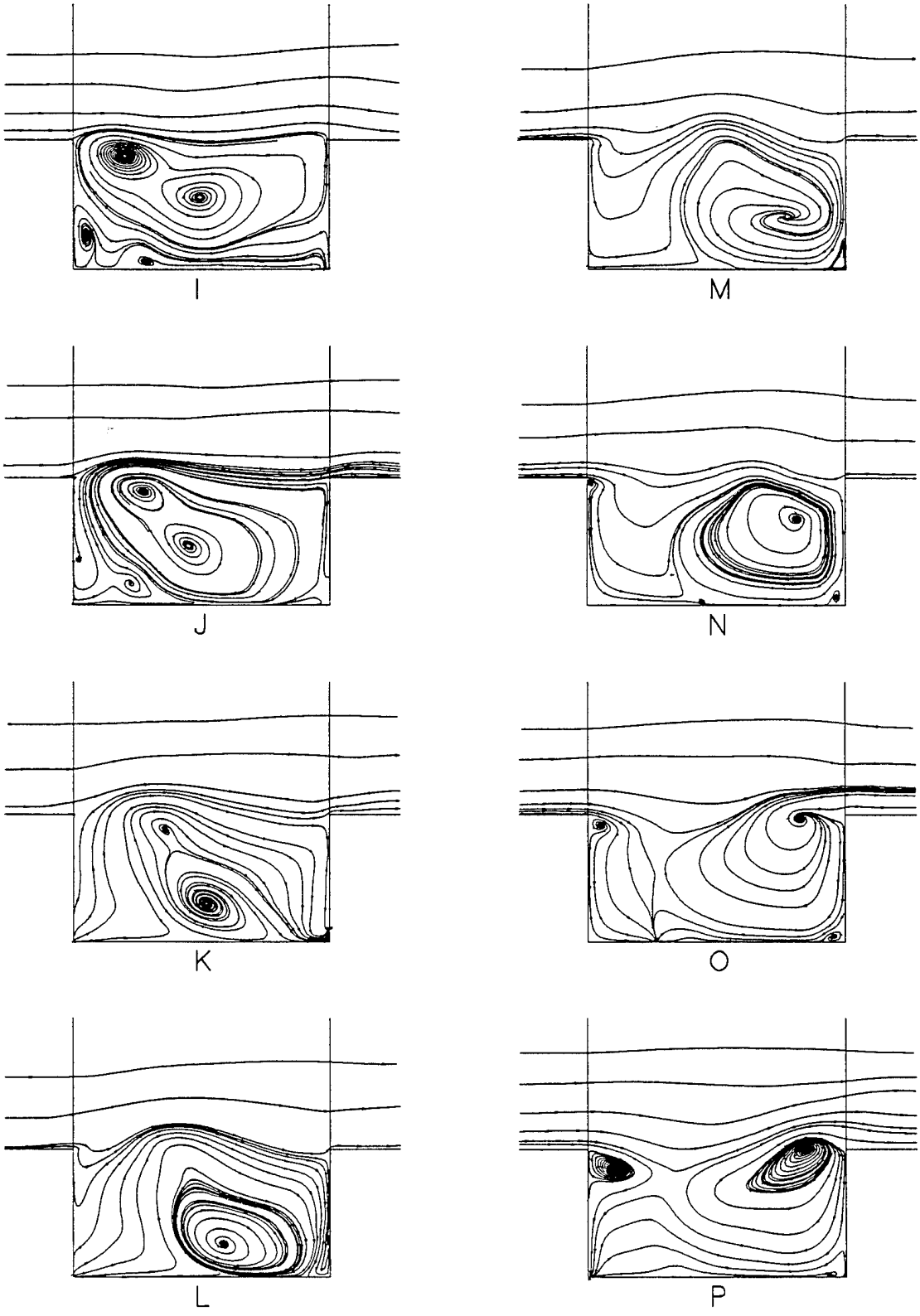

Time series streamline

Figure 1 (cont'd)

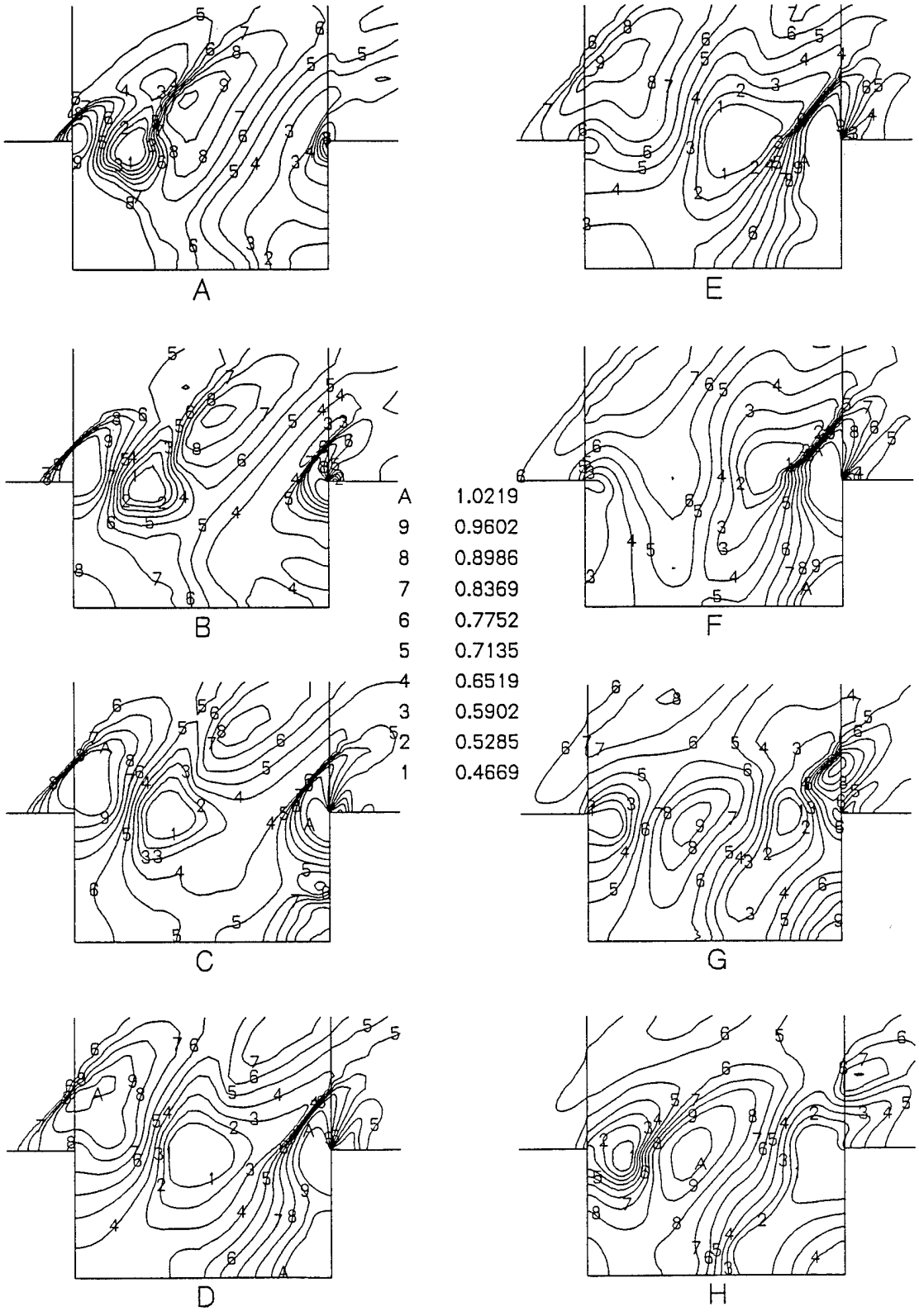

Time series pressure contour

Figure 2

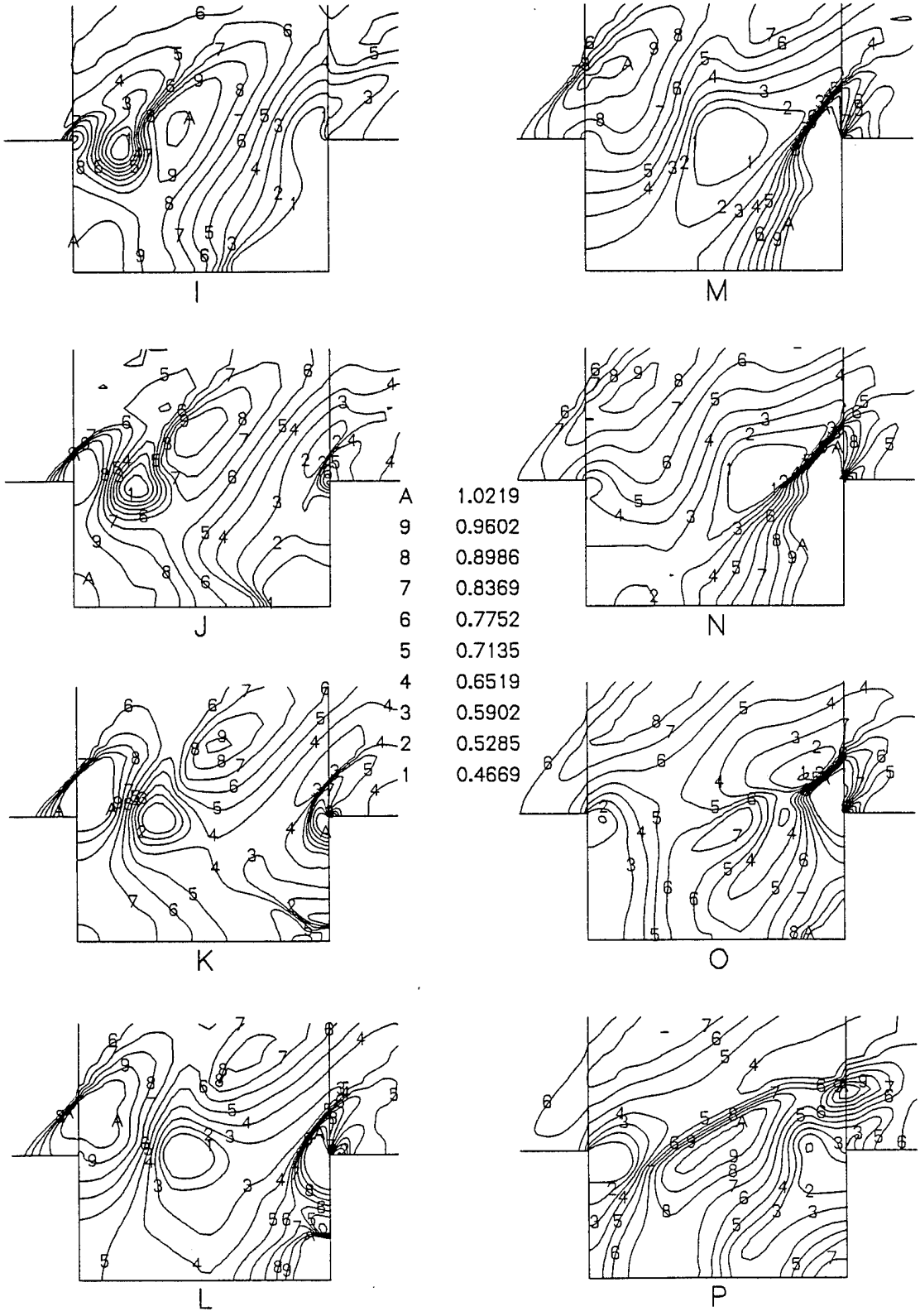

Time series pressure contour

Figure 2 (cont'd)

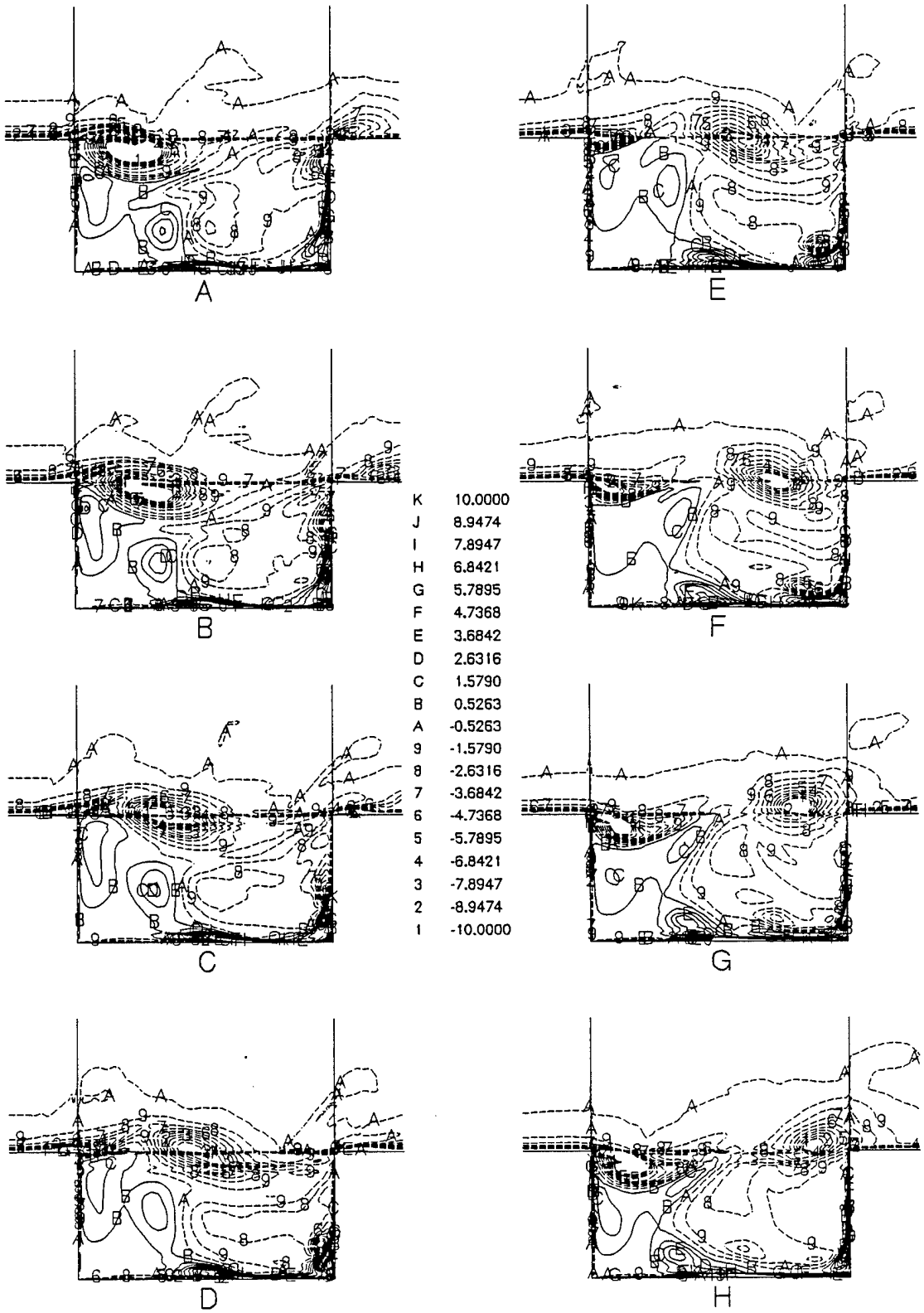

Time series vorticity contour

Figure 3

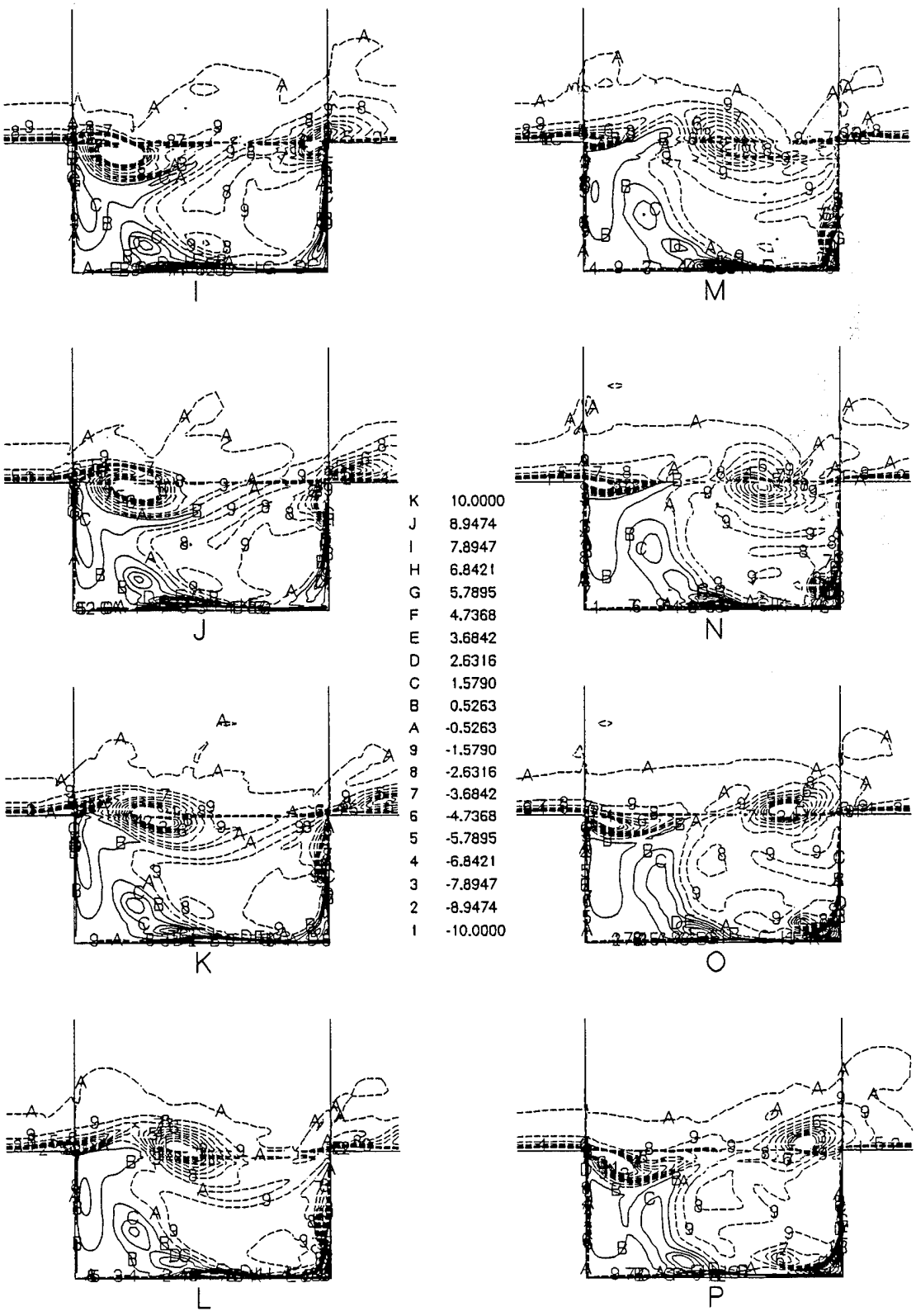

Time series vorticity contour

Figure 3 (cont'd)